DESIGN-CENTRIC METHOD FOR AN AUGMENTED REALITY ROBOTIC SURGERY

YANG LIANGJING
(B.Eng. (Hons.), NUS)

A THESIS SUBMITTED

FOR THE DEGREE OF MASTER OF ENGINEERING

DEPARTMENT OF MECHANICAL ENGINEERING

NATIONAL UNIVERSITY OF SINGAPORE

2010

Acknowledgements

This thesis is submitted as a partial fulfillment of the requirement for Master of Engineering degree in the National University of Singapore. The work is carried out at the Department of Mechanical Engineering, NUS. The author wishes to thank his supervisor, Assistant Professor Chui Chee Kong for his patient guidance and remarkable mentorship. His supportive attitude towards new ideas motivated the author in taking great initiative in the project. The project would not have been possible without his committed supervision.

The author is also grateful to the clinical collaborators, Senior Consultant Dr. Stephen Chang from Department of Surgery, National University Hospital and his team of research assistants. Their clinical perspective often leads to deeper exploration into the issue at hand.

The team of staffs in Control and Mechantronics laboratory offered enormous support to the project in terms of professional guidance, administrative facilitation and technical support. They include Mr. Yee, Ms. Ooi, Ms. Tshin and Ms. Hamida. The author also wishes to acknowledge the effort of Mr. Sakthi for his assistance in machining work.

The author is thankful to fellow students and researchers in Control and Mechantronics Laboratory for enhancing his learning experience and sharing of their experiences which significantly improved the quality of this project.

List of Publications

Journal

S. K. Y. Chang, W. W. Hlaing, L. Yang, and C.-K. Chui, "Review: Current Technology in Navigation and Robotics for Liver Tumors," *Annals, Academy of Medicine, Singapore,* (Invited Review Paper).

L. Yang, R. Wen, J. Qin, C.-K. Chui, K.-B. Lim, and S. K. Y. Chang, "A Robotic System for Overlapping Radiofrequency Ablation in Large Tumor Treatment," *Mechatronics, IEEE/ASME Transactions on,* vol. 15, pp. 887-897, 2010.

L. Yang, C.-K. Chui, and S. Chang, "Design and Development of an Augmented Reality Robotic System for Large Tumor Ablation," *International Journal of Virtual Reality,* vol. 8, pp. 27-35, 2009.

Conference

T. Yang, L. Xiong, J. Zhang, L. Yang, W. Huang, J. Zhou, J. Liu, Y. Su, C.-K.Chui, C.-L. Teo, S. Chang, "Modeling Cutting Force of Laparoscopic Scissors" in *3rd International Conference on BioMedical Engineering and Informatics (BMEI'10)*. Yantai, China, 2010.

L. Yang, C. B. Chng, C.-K. Chui, and D. Lau, "Model-based Design Analysis for Programmable Remote Center of Motion in Minimally Invasive Surgery " in *4th IEEE international Conference on Robotics, Automation and Mechatronics 2010*, Singapore, 2010.

R. Wen, L. Yang, C.-K. Chui, K.-B. Lim, and S. Chang, "Intraoperative Visual Guidance and Control Interface for Augmented Reality Robotic Surgery," in *8th IEEE International Conference on Control and Automation 2010*, Xiamen, 2010.

B. N. Lee, P. B. Nguyen, S. H. Ong, J. Qin, L. Yang, and C. K. Chui, "Image Processing and Modeling for Active Needle Steering in Liver Surgery," in *Informatics in Control, Automation and Robotics,* 2009, pp. 306-310.

F. Leong, L. Yang, S. Chang, A. Poo, I. Sakuma, and C.-K. Chui, "A Precise Robotic Ablation and Division Mechanism for Liver Resection," in *Medical Imaging and Augmented Reality*, 2008, pp. 320-328.

Table of Contents

Summary

This thesis presents the design methodology, development and experimentation of an augmented reality (AR) robotic surgical system. A design centric approach to the development process of the AR robotic system where dynamism is introduced to the traditional design regime for task specific surgical applications is proposed. The effectiveness of this approach is investigated by the development of a robotic module for needle insertion with a novel manipulator design that addresses the clinical issues in large tumor treatment. The provision for integration of the robotic modules to the AR robotics system demonstrated the seamless transition from innovative concept to detail technicalities.

The development of this robotic system is motivated by the clinical challenge in the treatment of large tumor using radiofrequency (RF) ablation. As a single RF ablation is insufficient to destroy the entire tumor larger than 3.5cm, a technique known as overlapping ablation is practiced. The need to insert and reinsert the needle multiple times results in uncertainties compromising the effect and predictability of the treatment. A robot assisted surgical system for executing multiple RF ablation of large tumor is advantageous for its speed, accuracy and consistency. Other advantages offered by robotic RF ablation include minimizing radioactive exposure and overcoming visual restriction as well as spatial constraint for minimally invasive approaches like laparoscopic or percutaneous surgical procedure.

Methodical analysis using mathematical models is performed. Remote center of motion (RCM) is an important concept in the kinematics for robotic minimally

invasive surgery (MIS). Kinematic modeling of mechanism design for both programmable and mechanical RCM is studied. The programmable RCM represented by a generalized model based on closed-loop kinematic chain uses multiple joints coordination to maintain the isocenter of surgical tool manipulation. It provides a framework for implementing a model-based control scheme in robotic MIS. The kinematic models of machine-environment interaction and clinical tasks of the applications are analyzed to justify the problem specific design goals. Subsequently, the execution mechanism is engineered. This includes designing the motion control which consists of mechanism design, actuation and sensory hardware, and control software.

An efficient overlapping ablation planning algorithm is designed to work with the robotic needle insertion manipulator. The average computation time from reading the tumor surface coordinates to the output of joint trajectories is 5.9 seconds on a typical personal computer. This "Voxel Growing" algorithm automatically produces the multiple ablation targeted points according to the tumor's profile.

Experimental methods including extensive computer simulation, and ex vivo testing with porcine liver organs were used to assess the performance of the system. The structural length index calculated from the workspace volume is close to the optimal articulating arm and is much better than that of a Cartesian manipulator. There is also a high degree of tracking accuracy and needle path consistency. The results demonstrated the clinical viability of the proposed AR robotic system, and feasibility of the design centric approach for medical device design.

List of Tables

List of Figures

Chapter 1 Introduction

This chapter defines the objectives of the project and introduces background information relevant to the work. The scope of the work is also indicated in the final section of this chapter.

1.1 Objective

This work focuses on the design and development of an augmented reality robotic system for the treatment of large tumor. The eventual goal is to improve the accuracy, consistency and minimize the invasiveness of interventional medicine through the guidance of augmented reality and robot assisted procedure. In addition, the medical challenge of large tumor treatment is addressed.

1.2 Background

With the advancement in computer-based medicine, accurate diagnosis and precise pre-operative plans are available [1]. However, effective and consistent intraoperative execution remains a challenge. Surgeons are constantly faced with operation conditions that put them to extreme visual and dexterous constraints. The introduction of augmented reality creates a real time link between virtually constructed preoperative models and an intraoperative environment. This complements the visual capability of the surgeons. Coupled with robot assisted surgical system, operation can be executed with more consistency according to the surgical plan.

There are different options to the treatment of liver tumor. While resection of tumor surgically is by far the best option [2] for liver tumor, only 20% of liver cancer

patients are suitable for open surgery [3]. Among the non-resectional procedures [4], RF ablation appears to be the most accepted treatment for liver tumors in terms of safety, ease of procedure and consistency [5, 6]. Radiofrequency (RF) needle ablation is a treatment technique that denaturizes tumor with heat created from ionic agitation generated by a needle electrode [4]. This form of treatment is a good alternative to liver resection.

However, complete annihilation of the tumor is dependent on the ablation volume coverage. In the treatment of large tumor with diameter that could be as large as 150mm, a single RF application is insufficient to destroy the entire tumor. Hence, multiple needle deployments and insertions are required. There are many researches on treatment strategies using multiple overlapping ablations [7-10]. Most of these researches revolve about planning and optimizing the ablation coverage to maximize effectiveness of the treatment. Although these developments significantly improve the effectiveness of pre-operative plans, achieving consistency and precision in intraoperative execution is non-trivial. The technique of multiple needle insertions for overlapping ablation is difficult to perform manually. Surgeons are often deprived of visual information or have to rely on non-intuitive image guidance in executing the preplanned ablation model. Performing such operation manually will also be subjected to uncertainties and inconsistent outcomes [8]. These clinical challenges coupled with the critical need for consistency motivates the development of intuitive AR image guidance and robot assistive devices specialized to facilitate such treatment technique.

1.3 Scope

An augmented reality robotic system is proposed for the treatment of large liver tumor. This thesis covers the methodology adopted for the development of an AR robotic system. The development process is demonstrated in the following chapters.

Chapter 2 surveys on relevant topics that provide background knowledge and an in-depth discussion on the state of the art technologies. This sets the conditions for identifying the design requirements which in turn facilitate conceptualization.

A design centric approach will be presented in Chapter 3 with the introduction of the developed AR robotic system and its components. Subsequently, the theoretical and engineering aspects of the design process are presented.

Chapter 4 elaborates on the kinematic modeling and mathematical principle behind the design analysis. The section on inverse kinematics discusses an effective computational scheme which tapped on the design advantages of the needle insertion manipulator.

After the establishment of a mathematical model, Chapter 5 reports on the path execution principle and implementation issues. This also includes technical discussion on mechanical hardware engineering and system software development.

Chapter 6 discusses the sciences and theories behind the proposed robotic AR approach for medical intervention. Discussion on intraoperative registration and robotic navigation are presented. An operation workflow is introduced at the end of the chapter.

The execution of medical interventional application is demonstrated in Chapter 7. Robotic multiple overlapping ablation is proposed to address the medical issue of large tumor treatment. An overlapping ablation planning algorithm was developed to provide automatic preoperative ablation plan.

Chapter 8 reports and discusses the performance of the system. The discussions include computation and simulation based evaluations. Experiments are also carried out. The outcomes of two ex vivo studies are documented.

Finally, the thesis concludes with recommendation for future development in Chapter 9. Future directions and potential developmental follow ups are identified based on the findings and accomplishment of this thesis.

Chapter 2 Literature Review

Due to the interdisciplinary nature of the project, the literature review involves a wide range of relevant topics in both engineering and medical fields. Discussion on classical robotic design and background information of medical intervention were presented. This is followed by a survey on current state of the art technologies and contemporary researches in relevant fields.

2.1 Robotic design

2.1.1 Guideline for robotic design

Robotic design concentrates on the degree of freedom, physical size, load capacity, and the kinematic requirement of the end effector [11]. It is important to consider the range of tasks required by the application. While robotic design involves an understanding of the task requirements, it is not uncommon to have uncertainty in the task specification. As a result, design criteria were established as general guidelines in a typical robot design process. Like most mechanical system design, robotic design is usually not sequential but iterative in nature. Nevertheless, the main design processes include the various phases listed as follows [12].

1. Define topology of the kinematic chain

   In this step robot designer will decide on the nature of the multi-link system that made up the kinematic chain. It can be in the form of serial, parallel or hybrid type. Subsequently, the joint type will be determined based on the mobility

requirement. In-depth technical discussion on the selected kinematic chain topology will be discussed in Chapter 4.

2. Establish robot architecture

The robot architecture is defined by specifying the geometric dimension. For serial manipulator, Denevit-Hartenberg convention can be used to obtain the kinematic description of the manipulator system based on the robot architecture. The forward kinematics is usually expressed as an analytical function of the joint variables to describe various pose of the robot. This approach is used extensively for systematic analysis of the robotic kinematics and dynamics in this project.

3. Structural dimensioning for static load requirement

The link and joint parameters are sized according to the torque and force requirements of the robotic task.

4. Structural dimensioning for dynamic load requirement

The consideration is further extended to dynamic loading where the inertia effect of the manipulation system is analyzed as well.

5. Elastodynamic dimensioning

This procedure includes the consideration of the actuator dynamics.

6. Actuation and sensory system

Careful selection of the sensor, actuator and mechanical transmission mechanism is required to cope with task uncertainty during operation condition. As the dimension of the electromechanical components is often in reality related to the specification, designing the actuation and sensory units is non-trivial. This is because the system dynamics is usually affected by the physical attributes of the

hardware. It is not uncommon to execute several iterations before an optimal sizing of the electronics can be materialized.

2.1.2 Workspace specification

Workspace is an important consideration for robotic design as it defines the kinematic capacity of the robotic mechanism. The reachable workspace includes the region where the end effector of the mechanism can position regardless of its orientation. The dexterous workspace on the other hand took into account the orientation requirement of the end effector. Hence, the workspace of a manipulator specifies if a solution exists for a given task. Workspace analysis specific to the needle insertion manipulator will be discussed in Section 4.1.

2.1.3 Computer-aided design for robotics design

Computer-aided design (CAD) has been introduced to the traditional approach of robotic design. The conventional approach with heavy reliance on experimentation and trial prototyping is made more efficient with CAD implementation. As the general robotic system evolve to take on more sophisticated roles, CAD for robotic design are extended beyond the field of industrial robots. Vukobratovic *et al.* [13] explain the process of CAD in robotic design using Total Computer-Aided Robot Design (TOCARD) system developed by Inoue *et al.* [13]. The design procedure constitutes three design systems including fundamental mechanism, inner mechanism and detailed structure.

2.2 Surgical intervention

RF treatment can be executed in three modes of surgery. Listed in increasing order of invasiveness, they include percutaneous insertion, laparoscopic procedure and open surgery. Laparoscopic and percutaneous intervention are minimally invasive techniques which aim to minimize the trauma imposed on the patient so as to yield better treatment outcome, shorter recovery time and minimize complications [14-16]. There is a clear shift in paradigm from the common practice of open surgery to laparoscopic surgery since the latter was first performed in 1985 [17]. Laparoscopic surgery requires incision of typically less than 10 mm for the entry of surgical tools into the abdominal cavity via trocars [18]. The workspace within the inflated abdominal cavity is maintained by carbon dioxide while a laparoscope is used to acquire vision in the surgical site. Images are subsequently transmitted to a high resolution monitor for display.

However, minimally invasive procedures are difficult to execute as surgeons are subjected to visual and dexterous constraints. Surgical instrument manipulation within the operation site during a laparoscopic surgery has a reduced mobility of 4 degree of freedom (DOF). Currently, surgeons have to rely on image guidance technology to navigate their surgical tools and RF needle. Though laparoscopic images depict the abdominal cavity on a high definition monitor, the perception is often handicapped due to the two dimensional nature of the view. Moreover surgeons have to rely on their judgment based on diagnostic images and intraoperative spatial awareness to successfully target a tumor embedded in the liver.

2.3 Computer-aided surgery

Computer Aided Surgery (CAS) refers to the use of computerized procedures to facilitate surgical planning, execution and follow-up. The principal goal is to improve medical results with accuracy and minimal invasive execution. It was initially an approach which integrates various computer imaging techniques and digital technologies to complement surgical treatment [19]. As a result of its interdisciplinary nature, the scope of CAS eventually expanded to form the basis of promising technologies like intraoperative image guidance, surgical navigation system, robot assisted surgery and telesurgery. Presently researches in CAS have evolved to cover cross-disciplinary fields which further intertwine with minimally invasive surgical techniques, interventional devices and biomechatronics. A CAS system can include but not limited to components like image guidance, surgical navigation, or robotic assistive modules. Taylor and Kazanzides termed the computer-based surgical system as computer-integrated interventional medicine (CIIM) [1]. The general architecture of the described CIIM system includes the following.

1. Computational units for image processing, surgical planning and monitoring
2. Databases of patient-specific information
3. Robotic devices
4. Human-machine interface relating virtual reality of computer representation to actual reality of the subject, interventional room and clinician.

In spite of the sophistication in contemporary CAS system, it essentially bears two principal roles which include intuitive navigational guidance and dexterity support including stabilizing intended motion.

This thesis proposed the application of AR for intuitive visual guidance and robotic module for manipulation of surgical tools and equipment. The proposed AR robotic surgical system comprises a rectangular robot for direct projected AR and robot assisted needle insertion through computer planned ablation model.

2.4 Robotic needle insertion

Research and development of robotic applications for interventional medicine have made great advancement. There are works involving robotically assisted needle insertion system for prostate biopsy and therapy with intraoperative CT guidance by Fichtinger *et al* [20], and ultrasound guided needle insertion robot by Hong *et al* [21]. An example of needle insertion treatment is RF ablation. The RF needle is an electrode that punctures soft tissue to reach the target. The tip of the needle creates a volume of ablation as a result of local resistive heating caused by agitated ions [5]. As the tissue goes beyond 60^{o}C, cellular death results and eventually forms a region of necrosis. Typically the ablation region should be 10mm beyond the actual size of the tumor as safety margin to ensure effective ablation of tumor [4]. As a result of the RF needle limitation in ablation capacity, tumor larger than 3.5cm usually requires multiple placements and/or deployment of needle which often compromise on the effect and predictability of the treatment [8, 18]. As a result many researchers proposed the use of surgical robotic modules for needle insertion. Du *et al.* developed

a 5 DOF robot manipulator for RF needle insertion [15]. He further researched on the control system and the robotic technologies for ultrasound image guided RF ablation [22, 23]. Unfortunately, these developments of robotic system focus on single RFA and cannot fulfill the requirements of multiple overlapping ablations. Robotic assisted needle insertion aids rapid re-targeting for multiple ablations and optimizes distribution over a treatment volume by executing a precise path plan [24]. Without the robotic system, the procedure can be difficult to execute or impossible using manual execution.

2.5 Augmented reality surgical system

Despite the advancement in robotic technologies, the entire procedure of a general surgery remains too complicated for robots to handle with absolute autonomy. Hence robotic modules are considered components of CAS instead of a standalone solution. Image-guided surgery with AR platform empowers the surgeons with visual feedbacks in a more realistic and intuitive interface. This enhances judgment and leads to more desirable outcome [25, 26]. Procedure requiring judgments from surgeon like selection of incision sites, surgical tools navigation, path planning etc can be complemented through Augmented Reality (AR) guidance.

Recently, there have been enormous efforts in the field of AR and robotics for surgical applications [25-40]. AR usually involves the integration of virtual realistic model into real time view of the scene [28]. In the surgical context, an AR system enables the overlay of supplementary visual information in surgeons' real perspective [41]. This can be implemented through various forms. They include the use of head-

mounted device (HMD) [25, 40, 42], AR window [27], image overlay onto classical screen-monitor [34, 38] or direct-projected AR [33, 36, 37, 39, 43]. The direct-projected AR platform has the capability to address some of the current AR technological limitation. It offers advantages in the field of view. In addition, the ergonomic ease for the user is in alignment with our user centric design approach.

The principle behind the implementation involves registration of pre- and intra-operative data to real world perspective [25, 44]. A challenge especially difficult to tackle in surgical AR application is the issue of large deformation in soft tissue. This has led to relatively slower development in the cardiac and gastrointestinal surgery compare to that of neural and orthopedic [41]. As a result, research in this field is in close relation to that of tissue-tools interaction modeling. The subsequent section will be a brief review in this research topic.

2.6 Modeling and simulation of needle insertion

An accurate interaction physic-based model is vital for the performance of the AR system. Modeling and simulation of needle insertion is useful for designing robotic liver needle insertion and ablation system. Its potential contribution to the advancement of robotic guided needle insertion was recognized with numerous publications on the development of various simulation models for research purposes, training tools or clinical implementations. A simulation model based on measured planar tissue deformations and needle insertion forces is developed by DiMaio *et al.* [45]. Computer simulation in needle insertion eventually fuels the development of optimization RF ablation. One recent achievement in this subject is the development

of an algorithm for trajectory optimization in three dimensionally visualized computer assisted surgery by Baegert *et al.* [10]. This is a significant work that realizes automatic computation of optimal needle insertion that is executable in computer integrated robot assisted surgery. Villard *et al.* [46] proposed a real-time simulation and rapid planning tool, RF-sim dedicated to RF Ablation of hepatic tumors that allies performance and realism, with the help of virtual reality and haptic devices. The planning tool performs optimal placement planning with a developed set of algorithm. Generally, it uses an iterative method to formulate the minimal volume. Simulated annealing method was used to locate the best needle positions subsequently. The developed needle deployment strategies will be discussed under Chapter 6.

Chapter 3 Design

A design centric approach is adopted in the development of the AR robotic system. Innovations in design are introduced to address the clinical needs and operational requirements for the surgical application. The approach includes establishing the design requirement, design conceptualization, design for specification, prototyping and refinement.

However, the nature of the application required more than open-ended design innovations. Specific technical aspect requires substantial engineering analysis and systematic approaches as discussed in the literature review under Section 2.1. The entire process therefore, encompasses both technical novelties and scientific insights to the design issue. This chapter will give an overview on the major stages in the development methodology leaving the detailed technicalities and similar mathematical analysis to subsequent chapters. Finally, the last three sections will be dedicated to the introduction of the developed prototypical system.

3.1 Design considerations

Design considerations are the foundational procedure where research and information gathered are further organized and translated into design related issues. While medical robotics may inherently bear similar design issues as industrial robot design, there are functional requirements unique to it. Moreover, some guidelines on similar design issues may also be inapplicable in the implementation of surgical robotic system.

Safety is an important design consideration in all classes of robot. However, safety guidelines for industrial robot are not always applicable to surgical robot. Administrative risk control can be implemented for industrial robot through isolation of it from human operators when powered. This is however inapplicable in a surgical environment where both human operators and subjects cannot be excluded from the machine's workspace [47]. In view of that, a reliable mechanism to cut off the power during an emergency as a form of engineering risk control should be available. In an event of failure, the system has to be detachable from surgical tools easily to discontinue unintended motion or resume manual operation so as to minimize interruption to operation. This translates into safety design features like the quick release needle gripper and detachable end-effector featured in Fig. 1.

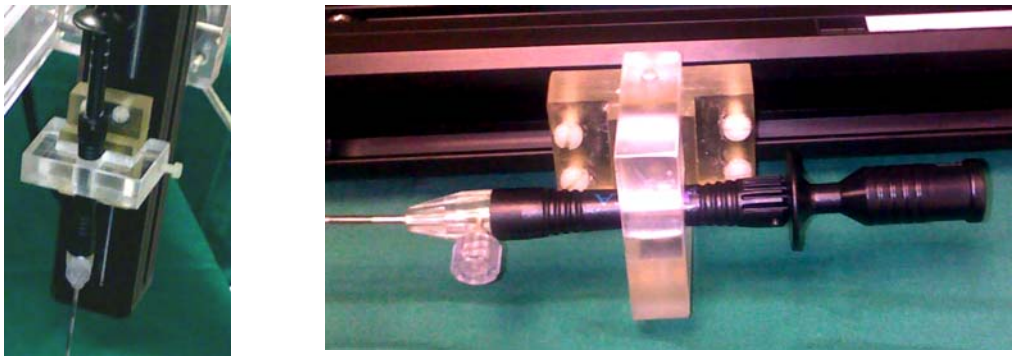

Fig. 1 Quick release needle gripper

Another consideration unique to surgical robots is the issue of sterilizability. The design should facilitate sterilization. Those parts having physical contact with patient need to be sterile. The most common method of sterilization is by autoclaving where devices are treated with pressurized steam. Hence material selection becomes an important design consideration. Metallic materials are used in surgery unless parts are

disposable. Electrical components may be sterilized using 70%-90% ethanol and irradiation with ultraviolet light. Apart from material selection, the modular approach as mention previously is helpful in the sterilization process. It accommodates sterilization of components especially the end effector which may contact the patient directly during an operation. Such component will be small enough to undergo sterilization in facilities like autoclave.

3.2 Design conceptualization

This process is a strategic phase of the entire development process. From the various design considerations discussed previously, design strategies can be formulated and design goals established. In the early development stage, this includes the construction of system schematic to facilitate mathematical analysis. Subsequently mathematical models are derived based on joints kinematics within the workspace of the system and specification of the necessary design parameters. Details on the technicalities of the kinematics modeling are discussed in Chapter 4.

An actual design plan can be further conceptualized by the use of Computer Aided Design (CAD) software after a mathematically feasible concept is being constructed. The establishment of the CAD models of the mechanical system enables visualization of the design. In addition, it provides a basis for subsequent prototyping and refinement process.

Mathematical analysis was done in computational software, Matlab^{TM} and a specialized toolbox, Robotics toolbox [48]. The Toolbox was used to construct the conceptualized manipulator structure as a virtual object. The library of functions

available facilitates the mathematical analysis of the robot kinematic architecture. Fundamental operations including configuration synthesis, inverse kinematics, workspace analysis etc can be executed on the constructed virtual manipulator object. Fig. 2 shows the implementation of various design concepts using CAD software. The next section will explain how initial design concepts are subsequently materialized as prototype and undergo physical design refinement.

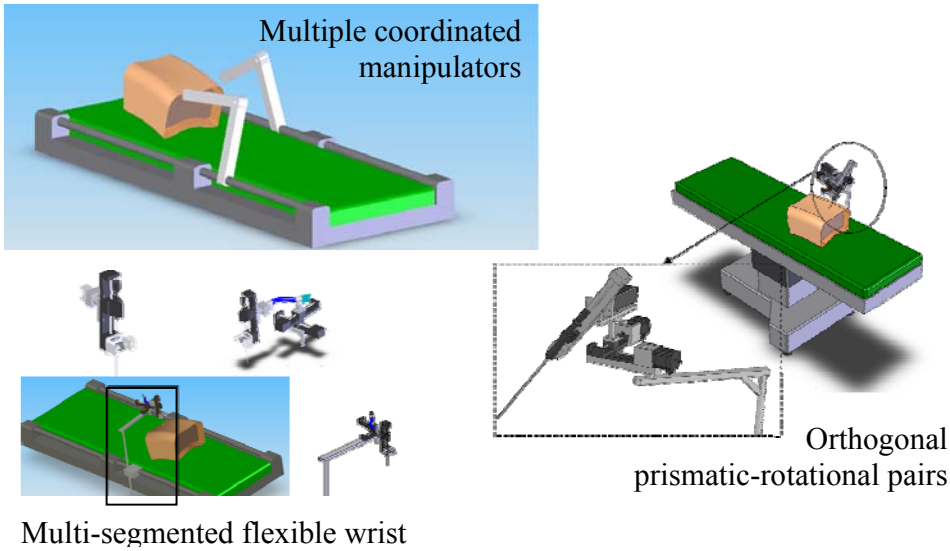

Fig. 2 Implementation of design concept in CAD software

3.3 Prototyping and refinement

Virtual models are implemented based on the derived mathematical models. These models are constructed in CAD software, Solidwork. The software environment facilitates rapid virtual implementation of a developed design concept. It also produces realistic visualization and provides design insights to implementation issues. The constructed CAD model is translated to models in simulation software tool,

SimMechanics™. Some of the intricate geometric and complex dynamic parameters can be difficult and tedious to define in simulation environment. With CAD software as the design environment and simulation software tools as the analysis platform, the entire modeling and simulation process is more efficient.

3.4 Overview of Augmented Reality Robotic System

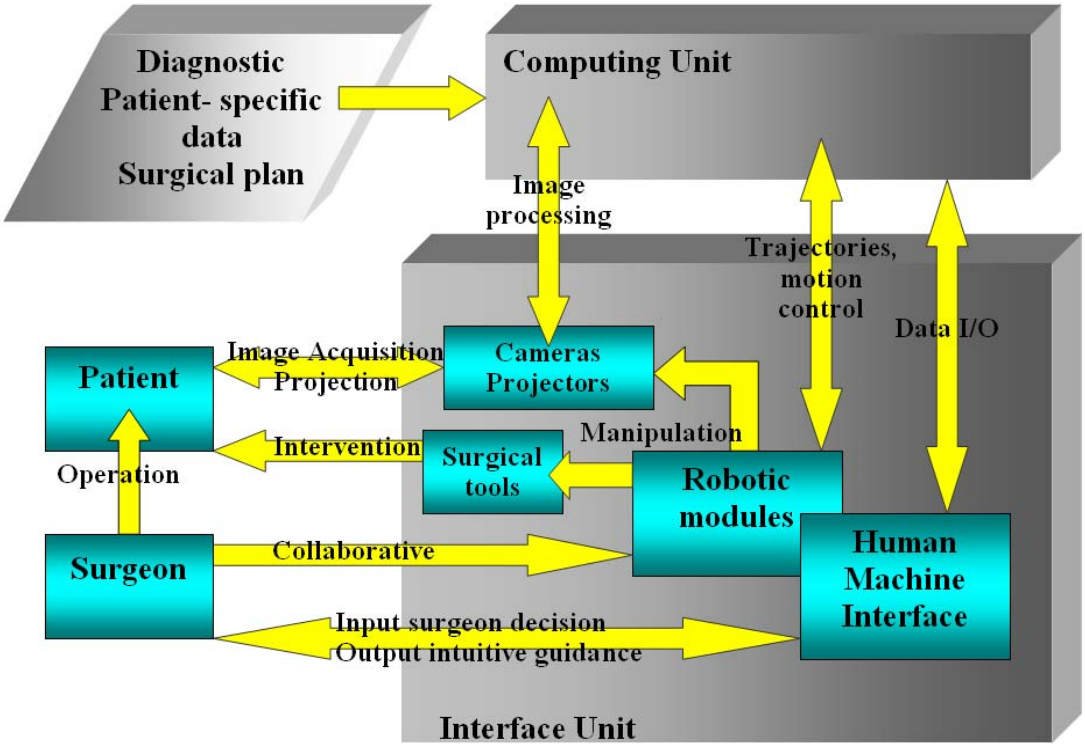

Fig. 3. System architecture of the AR robotic system

Fig. 3 illustrates the system architecture of the proposed AR robotic system. A secondary projector and stereo-camera system were introduced into the system to realize the intraoperation visualization and augmented reality control interface. Hence,

the current system consists of a rectangular robotic projector-camera system and a serial manipulator needle insertion robot. For a typical interventional treatment, patient-specific information obtained from preoperative diagnostic phase will be processed to derive the surgical task plan. Subsequently, this will be made available to the computer system responsible for controlling the interface unit for various intraoperative tasks like image projection, object tracking, robotic path planning, command execution etc. The primary projector is responsible for the projection of the patient specific anatomical images including the relevant organ and vasculature network acquired from medical scans and image processing. The secondary projector displays dynamic overlay of needle image intraoperatively. This overcomes the barrier of visual constraint and projection occlusion during percutaneous or minimally invasive procedure. The secondary projector performs an active role by displaying the actual needle path executed by the robot under the control of the surgeon and indicates the region of necrosis resulted from each insertion. In addition, an interactive control interface for the surgeon to manipulate the AR images and robotic module is under development. This feature uses the hand gesture as an input for a more intuitive HCI. Fig. 4 is an illustration of the enhanced AR robotic workstation.

The direct-projected AR platform was implemented to demonstrate our proposed AR robotic system. This mode of AR has the capability to address some of the current technological limitation in AR application as mentioned in the literature review. The key reason is the ergonomic advantages for the user which is in alignment with our proposed user centric design approach.

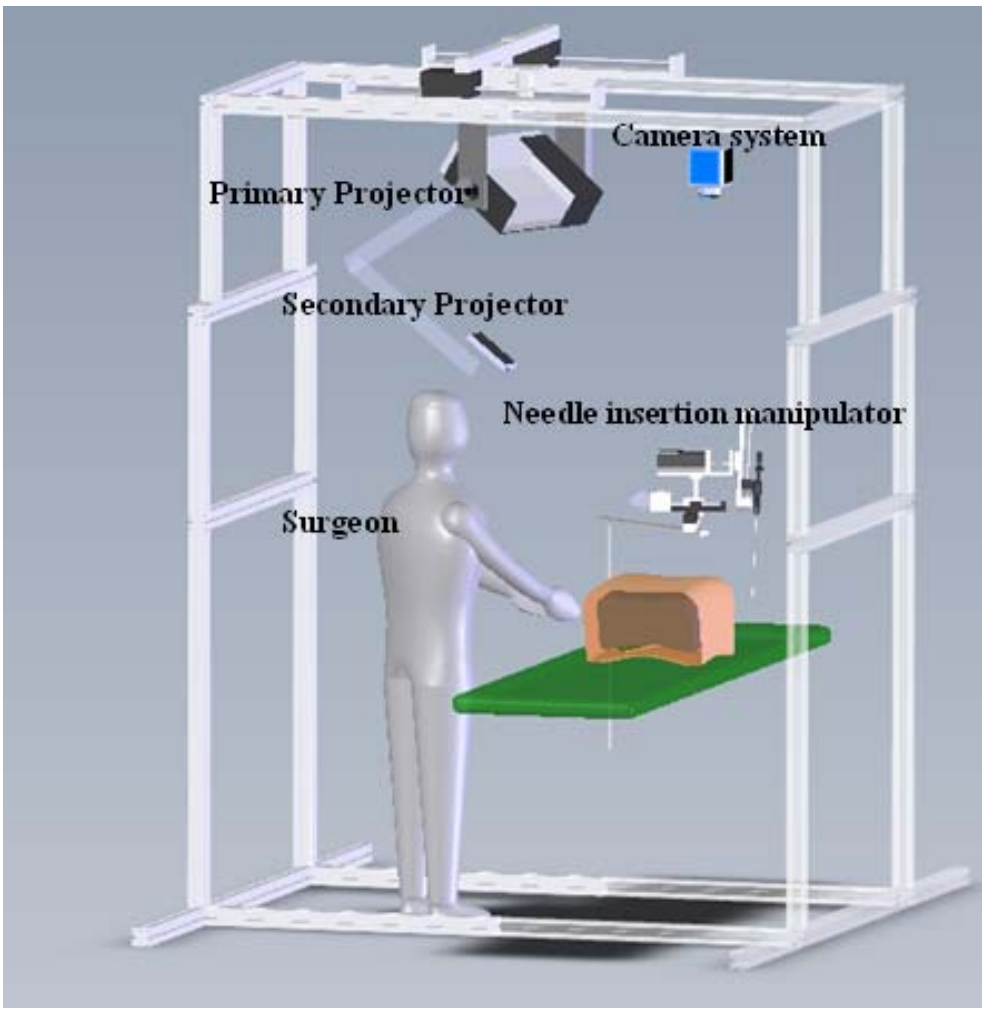

Fig. 4. Enhanced AR robotic workstation

The projection system consists of aluminum profiles assembled structural frame and an adjustable projector housing. The upper frame can be dismantled from its base and mount onto ordinary workbench for our current development and testing of the AR system. Fig. 5 illustrates the testing workbench where motion accuracy and image projections are tested. Motion control is implemented with ball-screw translational stages and motorized mechanism driven by fine resolution stepper motors. Apart

from motion control, the motorized mechanism provides geometrical awareness to the system for tracking purpose. This will be discussed in Section 5.2.

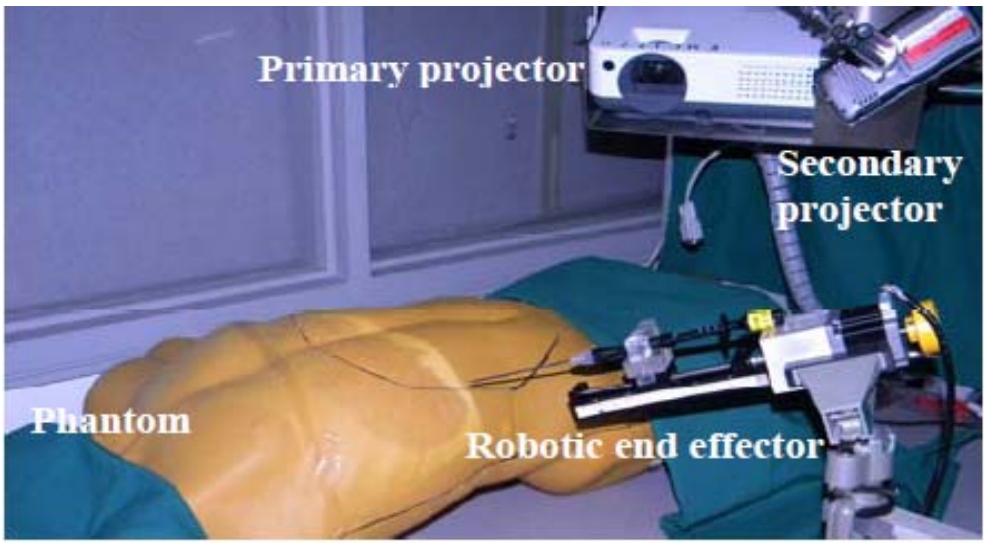

Fig. 5 Testing workbench with phantom human model

A novel manipulator mechanism design for multiple overlapping ablations is developed. This specialized robotic arm is an 8 DOF serial manipulator comprising of 3 passive links and 5 motorized axles. This structural mechanism is illustrated in Fig. 6. The novelty of this robotic design lies in its large tumor treatment application. It adopted the concept of a micro-macro approach within a manipulator mechanism. This design concept is similar to the micro manipulator mechanism defined by Craig [49].

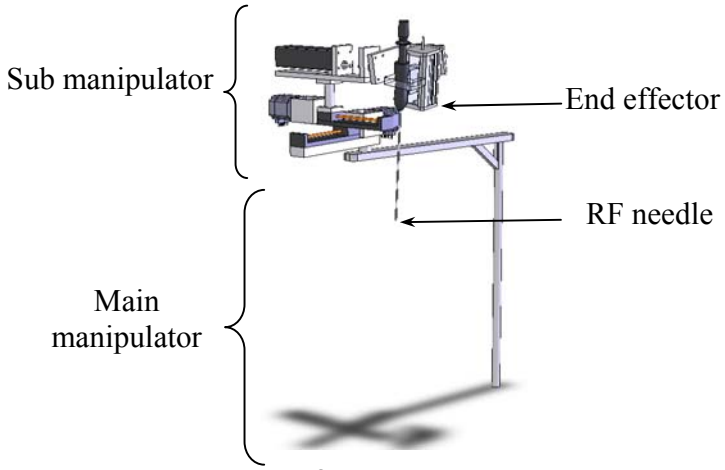

Fig. 6 CAD model of manipulator in surgical system

The first 3 passive links make up the main manipulator responsible for deployment of the needle to an initial position. It is designed in a SCARA-like configuration which manipulates the sub-system in a cylindrical workspace. The 5 DOF sub-manipulator system located at the distal end is dedicated to multiple needle insertions process and capable of dexterous manipulation for obstacles avoidance. It is also designed to perform RCM manipulation during minimally invasive surgery (MIS).

The articulated nature of the manipulator structure is advantageous for navigational trackers implementation. Wireless orientation sensors are used for tracking of the serial manipulator. Cartesian coordinates can be obtained easily by applying the appropriate Jacobian transformation without having to resort to expensive technologies like active optical triangulation systems, ultrasound localizers or general computer vision system. Apart from the technical advantages, this design also facilitates efficient computational scheme for inverse kinematics. This will be obvious in our discussion in Section 4.4.

The sub manipulator can be dismantled from the main manipulator. This is illustrated in Fig. 7.

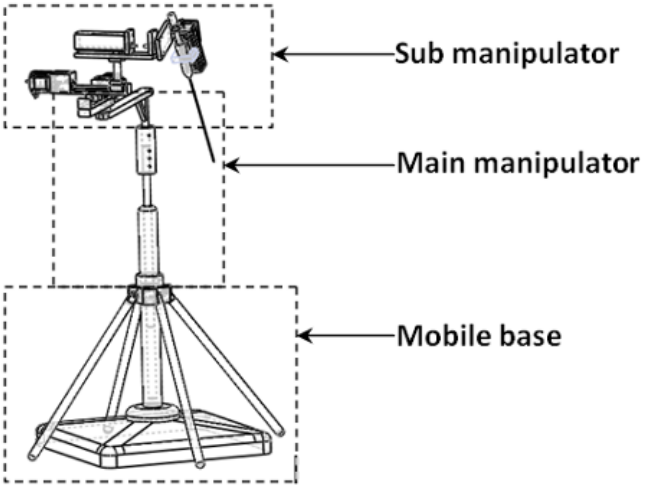

Fig. 7 Mounting of robotic manipulator to stable mobile base

The entire robotic manipulator can be mounted on to a wheel mobile base. Once the mobile base is at the desired position, support stands at the stem can be deployed to ground the base firmly. This design resolves the conflicting criteria for mobility and stability. In addition, the supporting point of the support stand can vary along the stem with respect to the fix elevation of the manipulation. The feature makes stability adjustment independent of the structure height. As such the designed base is less space intrusive compared to conventional tripod. This is an important operation requirement in the space constrained surgical theater. Fig. 8 shows the physical implementation of the robotic mechanism.

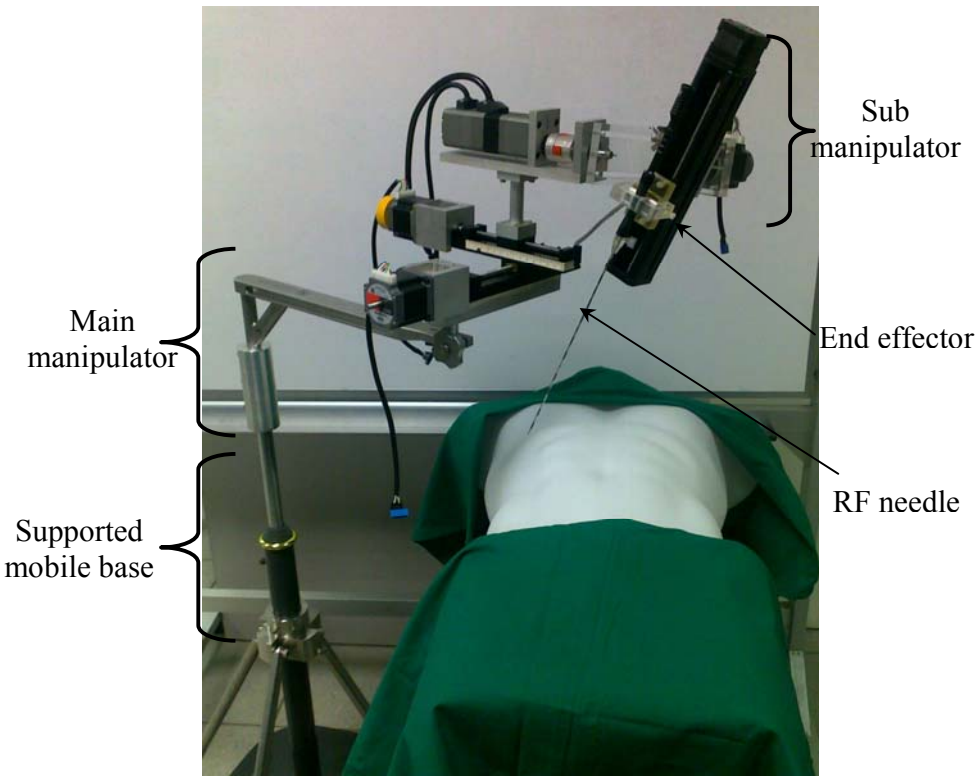

Fig. 8 Prototype of robotic needle insertion

Chapter 4 Robot Kinematics

The design centric development process integrates substantial methodical analysis through a mathematical model-based approach. This chapter discusses the construction of a kinematic model for mathematical analysis which is in turn translated to engineering specifications for mechanical system design. Kinematic models of machine-environment interaction and clinical tasks of the applications involved are analyzed to justify the problem specific design goals involved in this clinical application. The technical discussion on the principle of the path planning and engineering of control applications is subsequently presented.

4.1 Kinematic requirement

It is common to have bones, vital organs or crucial vessels within the highly vascular liver obstructing the direct path to the target especially when multiple needle insertions are required. Therefore, the robotic system must be equipped with obstacles avoidance capability as illustrated in Fig. 9. This feature can be achieved through the implementation of kinematically redundant manipulator. As the application deals with rigid RF needle, the path of the needle after incision is assumed to be straight. Hence, given a target, there could be more than one path from the point of incision to the target. When a 14G needle is used, a uniform radial margin of 1.5mm will be established conservatively to provide clearance for the shaft of 2.11 mm in diameter. From a design point of view, the manipulator should have sufficient task capacity to position and orientate the needle such that it assumes the linear trajectory upon

incision. This feature comes in the form of dexterity. By maximizing the local dexterity of the robotic configuration, the potential mobility of the needle path is maximized.

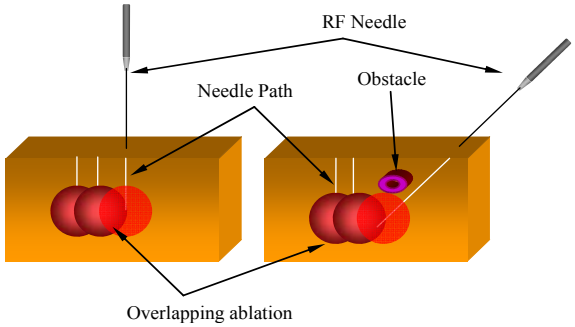

Fig. 9 Overlapping ablation technique

Kinematic redundancy further enables remote center of motion (RCM). This is a design feature that enables the pivoting of surgical tools via a constrained port opening during minimally invasive procedure. The RCM mechanism decouples rotation and translation motion of the surgical tools spatially away from the robotic end effector [1, 50, 51]. The kinematics requirement is very similar to that of obstacle avoidance. However, to pivot the surgical tools at the constrained point, higher order of differential kinematic analysis is required to achieve motion coordination. This can be achieved through mechanical means by structural design for joint motion compliance. Alternatively, it can be attained through software control of multiple joint trajectories coordination. Both approaches have their advantages and disadvantages.

From a clinical point of view, mechanical RCM is considered to be safer than programmable RCM as the latter relies solely on software to maintain the isocenter. In addition, mechanical RCM usually results in a simpler kinematic model for joint control. Since the design is physically constraint to the trajectory for RCM, the control scheme can be simplified to independent joint control. However, the functionality and performance of a programmable RCM mechanism design is generally more desirable. It offers constraint flexibility, greater manipulability and higher task capacity. A pure mechanical RCM will not have the option of extending its task space beyond the constraint. Moreover, programmable RCM can be readily implemented through open chain serial manipulator which is generally more space efficient. For the case of mechanically lock RCM, some form of close loop chain mechanisms are required leading to a larger structure and operational work envelope [18, 50-53]. This poses practical problem in a space constrained operating theater.

The conflict between functionality and operation safety was resolved through a programmable- mechanical RCM mechanism. By situating the wrist at the distal end of the manipulator, the manipulator has sufficient dexterity to orientate the surgical tools to comply with the constraint at the trocar. The decoupled nature of the wrist facilitates self-compliance of the maneuvered tool by simply disengaging the motors. This design enables surgeon to decide on the mode of control. The manipulator can either execute motion through programmed RCM or mechanical self-compliance RCM.

The workspace geometry of MIS can be analyzed by multiple frames assignments as in a multibody system. Frame 0 can be assigned at the constrained entry point.

Subsequently forward kinematics can be done to describe the tip of the tool according to the frame assignment as illustrated in Fig. 10. The operational zone of a laparoscopic tool is represented by the blue sphere. The upper hemisphere represents the required workspace for the manipulator end-effector whereas the bottom hemisphere depicts the effective reachable workspace of the needle tips. The links parameter and joints variables are tabulated in Table I. θ_1, θ_2 and θ_3 can be seen as the Euler angle of the laparoscopic surgical tool while *d* is the approach of the tool.

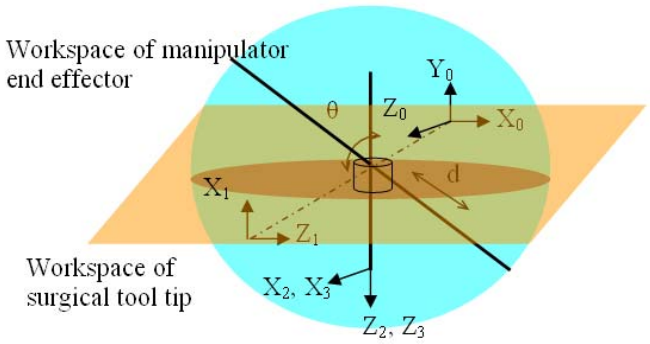

Fig. 10 Theoretical workspace envelope

TABLE I Denavit-Hartenberg table for fictitious links

	θ	D	r	α
${}^0T_1$	$q_1 = \theta_1$	0	0	90°
${}^1T_2$	$q_2 = \theta_2$	0	0	90°
${}^2T_3$	$q_3 = \theta_3$	0	0	90°
${}^3T_4$	0	$q_4 = d$	0	0

The forward kinematics can be worked out and expressed as homogenous transformation matrix as shown in (1).

$$
\begin{aligned}
{}^{0}\mathrm{T}_{4} &= {}^{0}\mathrm{T}_{3}\,{}^{3}\mathrm{T}_{4} \\
&= \begin{bmatrix} {}^{0}R_{3} = {}^{0}R_{4} & {}^{0}P_{4} \\ 0 & 1 \end{bmatrix} \\
&= \begin{bmatrix} c_1c_2c_3 + s_1s_3 & c_1s_2 & c_1c_2s_3 + s_1c_3 & d(c_1c_2s_3 + s_1c_3) \\ s_1c_2c_3 + c_1s_3 & s_1s_2 & s_1c_2s_3 + c_1c_3 & d(s_1c_2s_3 + c_1c_3) \\ s_2c_3 & c_2 & s_2s_3 & d(s_2s_3) \\ 0 & 0 & 0 & 1 \end{bmatrix}
\end{aligned} \tag{1}
$$

where $s_j=\sin(q_i)$, $c_i=\cos(q_i)$

Although the workspace requirement for laparoscopic surgery is illustrated in Fig. 10, not the entire region is relevant. Lum *et al*. [54] uses database analysis of 30 MIS applications on animal subjects to show that the surgical tool span over a region of 60^o cone centered at the opening for 95% of the duration. The reachable workspace requirement to cover the entire abdominal cavity requires the laparoscopic tools to have the mobility to move 90^o in the medial-lateral direction and 60^o superior-inferior direction. This workspace model is illustrated in Fig. 11. The inverted cone outside the abdominal cavity represents the required workspace of the end-effector. Laparoscopic surgical tools will maneuver within the abdominal cavity represented by the cone below the abdominal surface. Active robotic control of the manipulator end-effector is restricted outside the abdominal cavity because of the spatial constraint of the port's opening. The exceptions are micro-robot or active catheters [55, 56] which are beyond the scope of interest for this study.

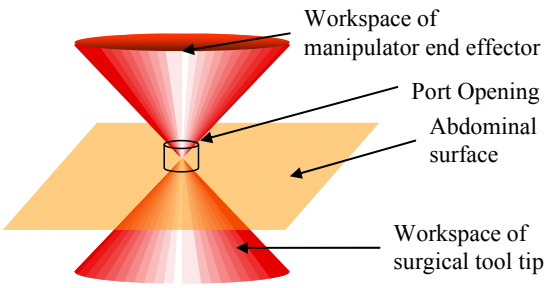

Fig. 11 **Practical workspace representation**

The empirically derived workspace requirement will be a reasonable guide for the kinematic requirement of the RCM. Our proposed manipulator design possessed the design feature of innately decoupled rotational and translational motion that enables the remote center of motion kinematics.

4.2 Analysis of RCM

4.2.1 Conceptualization

The derived mathematical model form the basis for model based design and analysis of RCM features. This is done with computation, modeling and simulation software tools. A closed-loop kinematic chain system will be used to model the design problem. The remote center is being analyzed as a mechanical constraint with 4 DOF.

Fig. 12 shows the schematic diagram of the system studied. The grounds are orientated facing up against gravity. This means that the manipulator has a base instead of being wall or ceiling mounted. Although this is not a requirement, the interest of this work focused on a general ground based serial manipulator. While mathematical solution of programmable RCM with ceiling mounted manipulator can

be trivial, actual implementation is difficult. It requires the operating theatre to be equipped with the necessary facilities specialized in such application. Hence, ground based serial manipulator was selected for seamless integration of robotic devices into the general setting of an operating theatre.

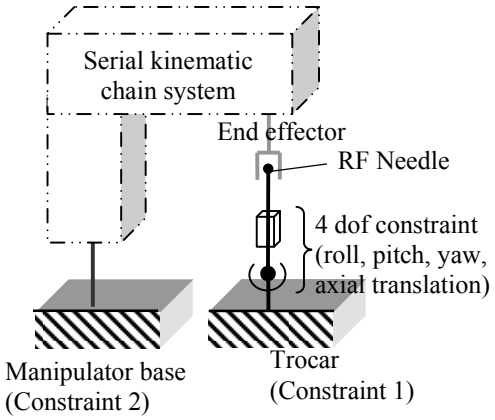

Fig. 12 Schematic model of design problem

Apart from the task kinematics requirement discussed previously, operational issues were considered. Traditionally, robotics modules take on an assistive role in collaborative mode rather than fully autonomous for the entire surgery [47, 57]. Hence a typical manipulator for assisted robotic surgical system possesses the option of passive component. Most existing programmable RCM mechanism relies fully on software multi-axis joint coordination [50, 58]. This approach did not decouple the insertion task with general manipulation. As a result, common surgical task like needle insertion may be a problem. To overcome this, the proposed design will situate the insertion stroke at the distal link so that the task of tool approach is decoupled from general manipulation of the tool. This leaves the remaining task degree of freedom the orientation of the tool about the incision port. The yaw motion

of the surgical tool is ignored as there is no need to orientate the needle about the axial direction of the shaft. Hence the remaining axis of control should be designed with mobility that fulfill the roll and pitch task degree of freedom while maintaining the constraint.

The remaining design criteria were based on geometric optimization theory proposed by Vijaykumar *et al* [59]. The manipulator structure will be decomposed into orientation and regional structure. Detailed illustration of the design can be found in Appendix A. The objective is to maximize reachable workspace and maximize the proportion of dexterous workspace within it. It was shown that the orientation structure is optimal when the axles are orthogonal. When the rotational axles intersect and are perpendicular, they are kinematically decoupled. In order to maintain the constraint through joint coordination, each of this revolute joint must be in serial to at least a prismatic joint. Hence these constitute two orthogonal pairs of prismatic-revolute joint as illustrated in Fig. 13. This figure is a schematic representation of the kinematic model of the sub manipulator suitable for programmable-mechanical RCM.

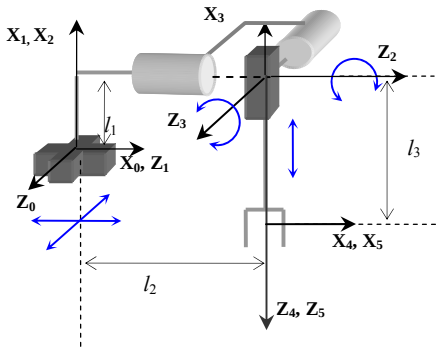

Fig. 13 Schematic representation of sub manipulator

4.2.2 Mathematical analysis

The kinematic model in Fig. 13 can be analyzed by assigning frames to links of the serial manipulator. Frames and link parameters are assigned based on Denavit-Hartenberg convention described by Fu [60]. Table II shows the joint variables and link parameters of the manipulator system obtained based on this convention.

TABLE II Denavit-Hartenberg table for sub manipulator

	θ	D	a	A
${}^{0}T_{1}$	90°	q_1	0	90°
${}^{1}T_{2}$	0	q_2	0	0
${}^{2}T_{3}$	q_3	l_1	-90°	-90°
${}^{3}T_{4}$	q_4	0	0	90°
${}^{4}T_{5}$	0	q_5+l_2	0	0

The transformation matrix of the needle tip (Frame 5) with respect to manipulator base (Frame 0) can be obtained by multiplying the homogenous matrix of each link. The governing kinematic equation of the sub manipulator can be represented by transformation matrix as shown in (2).

$$ {}^{0}T_{5} = \begin{bmatrix} {}^{0}R_{5} & {}^{0}P_{5} \\ \overline{0} & \overline{1} \end{bmatrix} \tag{2} $$

where

$$ {}^{0}R_{5} = \begin{bmatrix} -s_4 & 0 & c_4 \\ c_3c_4 & -s_3 & c_3s_4 \\ s_3c_4 & c_3 & s_3s_4 \end{bmatrix} \quad \text{and} \quad {}^{0}P_{5} = \begin{bmatrix} q_2 + c_4(q_5 + l_3) + l_2 \\ c_3s_4(q_5 + l_3) + l_1 \\ c_3s_4(q_5 + l_3) + q_1 \end{bmatrix} $$

Mathematical analysis was done using computational software, Matlab™ and a specialized toolbox, Robotics toolbox [48]. The Toolbox was used to construct the conceptualized manipulator structure as a virtual object. The library of functions

available facilitates the mathematical analysis of the robot kinematic architecture. MathScript code for the mathematical analysis is documented in Appendix B. Fundamental operations including configuration synthesis, inverse kinematics and workspace analysis can be executed on the constructed virtual manipulator object. Fig. 14 is a screenshot of the workspace generated using volumetric approach [61]. Piecewise calculus is used to generate the workspace of the conceptualized design.

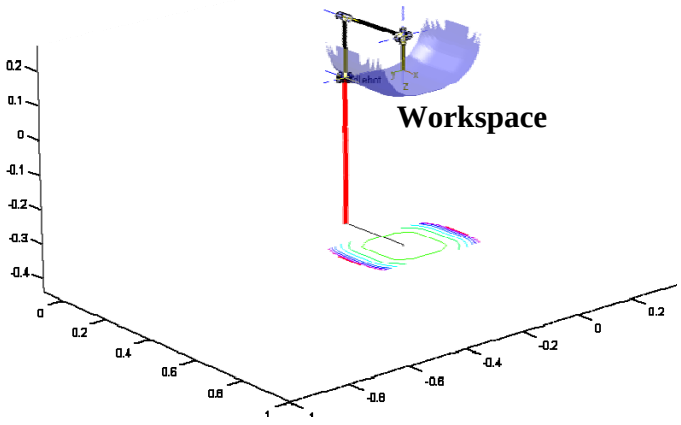

Fig. 14 Volumetric workspace of sub manipulator

4.2.3 Simulation

Virtual models are implemented based on the derived mathematical models. These models are constructed using CAD software, Solidwork. The software facilitates rapid virtual implementation of a developed design concept. It also produces realistic visualization and provides design insights to implementation issues. The constructed CAD model can be translated into virtual models in simulation software tool, SimMechanics^{TM}. This is an extended mechanical simulation software library in Simulink$^{TM.}$ Some of the intricate geometric and complex dynamic parameters can be

difficult and tedious to define in simulation environment of existing simulation software. With CAD software as the design environment and simulation software tools as the analysis platform, the entire modeling and simulation process is more efficient.

Fig. 15 depicts a virtual implementation of the conceptualized manipulator design based on the schematic drawn. In order to obtain accurate representation of the joint mechanism and spatial coordinates of the various components in the assembly model, special attention has to be taken in assigning the mating properties. The establishment of a virtual model facilitates simulation and analysis.

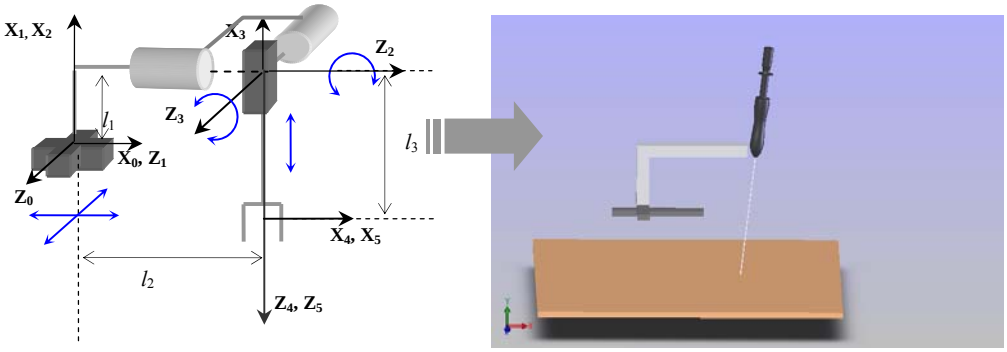

Fig. 15 Virtual implementation of design concept

Fig. 16 shows the block diagrams of the Simulink^{TM} graphical programming environment constructed base on the design architecture established during conceptualization. The respective physicals elements were labeled. The simulation environment allows the implementation of virtual actuation and sensory components for trajectory simulation and probing.

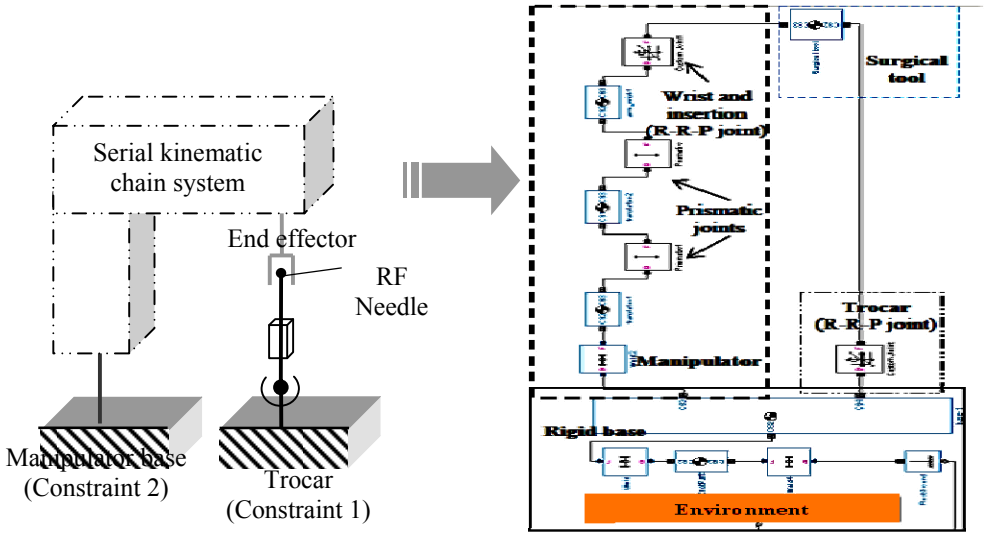

Fig. 16 Construction of virtual operation environment for analysis

Fig. 17 shows the simulation animation at four different time frames including t=0, t=9, t=18 and t=30. It can be observed that the RCM is being maintained at the circled region.

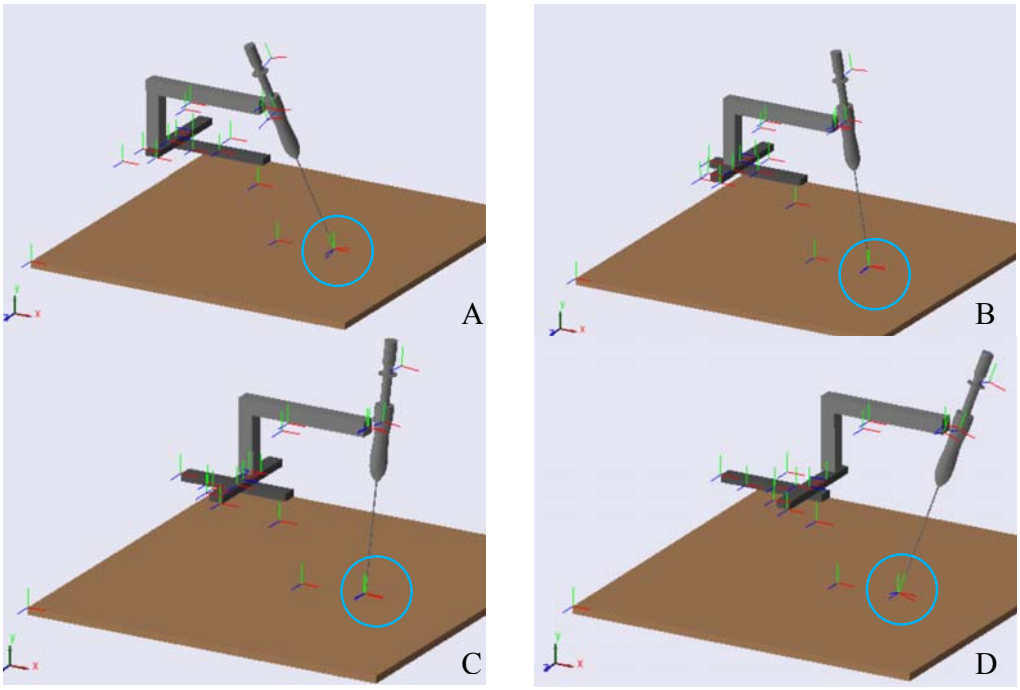

Fig. 17 Simulation of motion control in remote center of motion

4.3 Forward Kinematics

Forward kinematics involves the computation of geometrical position and orientation of components in multibody system. In this design centric approach, it is the foundation of many in-depth engineering analyses including design optimization, workspace analysis and model-based task planning. The forward kinematics also provides an implementation framework for coordinate transformation and registration in image guided AR applications. Similar to other form of mixed reality, interaction is an important concept in AR [25]. For effective link between virtual models and the real world spatially, some form of registration or calibration is essential. The pre-requisite to this procedure is the establishment of a kinematic model to the various interacting elements. The main mechanical components comprise of the projection system and the robotic needle insertion device. In the surgical system, components like the projector, camera, manipulator and RF needles are interactive elements. Hence, kinematic models are derived to represent these components spatially. In addition, the kinematic models describe the spatial interaction between components within the system thus providing a means for path planning and evaluation of the planned path.

The kinematics of the projector manipulation robot is described in [36]. Fig. 18 depicts the kinematic architecture of the projection robot. In essence, it consists of a Cartesian configuration with two axles of control to position the projector in a plane at a given height. There are two axles of control to orientate the projector in pitch and yaw fashion.

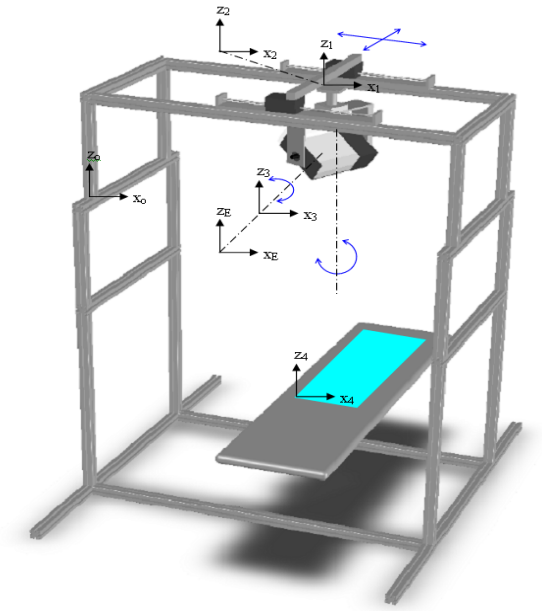

Fig. 18 Kinematic of projector structural frame

By multiplying the various transformation matrices, the homogenous matrix can be expressed in (3). The matrices include the planar translation on $z_1=d_1$ plane, θ_1 rotation in z_1-axis rotation, joint offset of d_2 in z_2 axis and θ_2 rotation in z_3 axis as shown respectively:

$$ {}^{0}T_1 = \begin{bmatrix} 1 & 0 & 0 & x_1 \\ 0 & 1 & 0 & y_1 \\ 0 & 0 & 1 & d_1 \\ 0 & 0 & 0 & 1 \end{bmatrix}, {}^{1}T_2 = \begin{bmatrix} c_1 & -s_1 & 0 & 0 \\ s_1 & c_1 & 0 & 0 \\ 0 & 0 & 1 & 0 \\ 0 & 0 & 0 & 1 \end{bmatrix}, {}^{2}T_3 = \begin{bmatrix} 1 & 0 & 0 & 0 \\ 0 & 1 & 0 & 0 \\ 0 & 0 & 1 & d_2 \\ 0 & 0 & 0 & 1 \end{bmatrix}, {}^{3}T_E = \begin{bmatrix} 1 & 0 & 0 & 0 \\ 0 & c_2 & -s_2 & 0 \\ 0 & s_2 & c_2 & 0 \\ 0 & 0 & 0 & 1 \end{bmatrix}. $$

$$ {}^{0}T_E = \begin{bmatrix} c_1 & -s_1c_2 & s_1s_2 & x_1 \\ 0 & c_1c_2 & c_1s_2 & y_1 \\ 0 & s_2 & c_2 & d_1+d_2 \\ 0 & 0 & 0 & 1 \end{bmatrix} \quad (3) $$

Fig. 19 is a schematic representation of the kinematic model of the needle insertion manipulator. It can be analyzed by assigning frames to links of the serial manipulator. As shown in Fig. 19, link 4 and beyond constitutes the sub-manipulator system. It manipulates precise motion of the needle guiding unit within the sub-manipulator

workspace. Frames and link parameters are assigned based on Denavit-Hartenberg convention described by Fu [60]. Table III shows the joint variables and link parameters of the manipulator system obtained based on this convention.

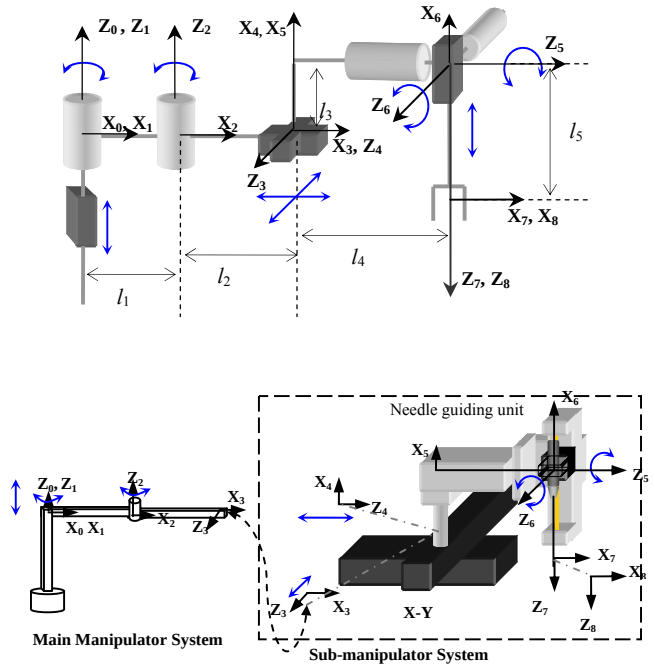

Fig. 19 **Schematic representation of manipulator kinematics partitioned design**

TABLE III: Denavit-Hartenberg table for manipulator

	θ	D	a	α
${}^{0}T_1$	0	q_1	0	0
${}^{1}T_2$	q_2	0	l_1	0
${}^{2}T_3$	q_3	0	l_2	90°
${}^{3}T_4$	90°	q_4	0	90°
${}^{4}T_5$	0	q_5	0	0
${}^{5}T_6$	q_6	l_4	-90°	-90°
${}^{6}T_7$	q_7	0	0	90°
${}^{7}T_8$	0	q_8+l_5	0	0

The governing kinematic equation of the manipulator can be represented by transformation matrix as shown in (4).

$$ {}^{0}T_{8} = \begin{bmatrix} {}^{0}R_{8} & {}^{0}P_{8} \\ \bar{0} & \bar{1} \end{bmatrix}, \tag{4} $$

where

$$ {}^{0}R_{8} = \begin{bmatrix} s_{23}s_6c_7 - c_{23}s_7 & s_{23}c_6 & s_{23}s_6s_7 + c_{23}c_7 \\ -c_{23}s_6c_7 - s_{23}s_7 & c_{23}c_6 & -c_{23}s_6s_7 + s_{23}c_7 \\ c_6c_7 & -s_6 & c_6s_7 \end{bmatrix}, $$

$$ {}^{0}P_{8} = \begin{bmatrix} s_{23}s_6s_7(q_8 + l_5) + c_{23}\left[c_7(q_8 + l_5) + l_4\right] + q_5c_{23} + q_4s_{23} + l_1c_2 + l_2c_{23} \\ -c_{23}s_6s_7(q_8 + l_5) + s_{23}\left[c_7(q_8 + l_5) + l_4\right] + q_5s_{23} - q_4c_{23} + l_1s_2 + l_2s_{23} \\ c_6s_7(q_8 + l_5)l_3q_1 \end{bmatrix}, $$

where s_j=sin (q_i), c_{ij}=cos(q_i), s_{ij}=sin (q_i+q_j) and c_{ij}=cos(q_i+q_j).

4.4 Inverse Kinematics

The 8 DOF manipulator is designed with kinematic redundancy. The inverse kinematics for this system is non-trivial. Obtaining joint variables for this type of system is notoriously tedious and computationally intensive. Although there are several optimizing algorithms based on numerical approach, they do not facilitate analysis of the design and mechanism. Moreover, the computational requirement is often too demanding for practical implementation. The computational load is an issue because of the need to compute inverse kinematics at a reasonable rate for execution of the path control-scheme. Hence, a closed-form solution is preferred for our problem-specific application. “Closed-form solution” in our context refers to the calculation of joint variables by analytical expression formulated through knowledge and understanding of the system. The computational strategy adopts a multiobjective systematic design approach. It makes use of the modular nature of the manipulator design to partition the complex task of needle insertion for overlapping RF ablations in a task dedicated manner. A set of optimal

solutions are subsequently obtained by means of sequential single-objective optimization of the two independent processes. The entire procedure can be decomposed into two independent subtasks namely deployment of sub-manipulator and multiple needle insertions for overlapping insertion technique.

4.4.1 Deployment of sub-manipulator

The needle is deployed to an initial strategic position defined by the planar centroid of the tumor geometry or position of the port in the case of laparoscopic procedure. This is done by the first 3 DOF of the main manipulator while the sub-manipulator treated as a rigid body. Closed-form solution for initial positioning of the needle can be obtained with simple geometric approach. The task of initial deployment of sub-manipulator is therefore closed-form-solvable and can be expressed as shown in (5) and (6). In laparoscopic surgery, the procedure can be used in tandem with optimal port placement technique [35, 62-64] and manipulator base placement technique [65, 66] for further effectiveness.

$$q_3 = \cos^{-1}\left[\frac{P_x^{\,2} + P_y^{\,2} - l_1^{\,2} - l_2^{\,2}}{2l_1 l_2}\right], \tag{5}$$

$$q_2 = \alpha - \beta \text{ if } q_3 > 0 ,$$

$$q_2 = \alpha + \beta \text{ if } q_3 < 0 \tag{6}$$

where

$$\alpha = \arctan 2(P_y, P_x) \text{ and}$$

$$\beta = \cos^{-1}\left[\frac{P_x^{\,2} + P_y^{\,2} + l_1^{\,2} - l_2^{\,2}}{2l_1\sqrt{P_x^{\,2} + P_y^{\,2}}}\right] .$$

4.4.2 Multiple needle insertions

The task of multiple needle insertions is executed by the sub-manipulator. The structure with the first 3 links from the main manipulator is seen as a rigid structure. Direct needle path will be taken in an obstacle-free insertion during an open surgery. This is a case of non-constrained manipulation. The effective ablation region is modeled as a sphere. Hence orientation of the needle tip does not have any effect on the ablation region geometry. The manipulator task space requirement reduced to a Cartesian (x,y,z) space. The inverse kinematics is straightforward as redundant Joint 6 and 7 take on constant values.

However, the kinematic manipulation is likely to be subjected to constraint. This is due to the present of obstacles in the robotic path and the spatial constraint imposed by MIS technique. In such cases the two degree of freedom redundancy comes in handy. A detailed computational scheme is designed to solve the inverse kinematic of the constrained system.

4.4.3 Computation scheme

This computation method is designed for the proposed task-specific needle insertion manipulator. It assigns the global frame of reference at the constraint. For a given set of target, a corresponding set of end-effector position can be obtained. The end effector position refers to the position of Frame 7 with respect to the global frame at the port. Hence joint coordinates (q_4, q_5, q_6, q_7, q_8) can be computed such that the needle is constrained within the entry port. The computational scheme is presented as follows:

Step 1: Compute end-effector position

For a given target P_T (x_T, y_T, z_T), find end-effector position P_E (x_E, y_E, z_E).

Since our application uses rigid needle, the corresponding end-effector positions can be obtained from the target points with the following transformation as shown in (7).

$$P_E = -I_k P_T \tag{7}$$

where

$$I_k = \begin{bmatrix} k & 0 & 0 \\ 0 & k & 0 \\ 0 & 0 & k \end{bmatrix} \text{ and}$$

$$k = \frac{z_E}{z_T}.$$

I_k is the scaling matrix. z_E is a constant determined during the deployment of the submanipulator discussed previously. The negative scaling matrix effectively maps the target position to the opposite octant of the 3D Cartesian space. This mapping relationship applies to transformation of the distal end to the proximal end of any general rigid laparoscopic tools.

Step 2: Obtain translational joint coordinate q_4 and q_5

By geometric inspection of the manipulator design, the following relationship of the joint and task coordinates can be observed:

$$\begin{pmatrix} q_4 \\ q_5 \end{pmatrix} = \begin{pmatrix} -y_E \\ x_E \end{pmatrix}. \tag{8}$$

Step 3: Obtain joint coordinate q_6, q_7 and q_8

As discussed previously, the remote center of motion can be analysis as a multibody system with 4 DOF. For analysis needle application the orientation along the axial

direction of the needle shaft is not relevant. Hence the motion of the end effector with respect to the global frame is analyzed as 3 degree of freedom motion including rotation along X and Y axis, and translation along the axial direction of the needle shaft. Mathematically, this can be represented by a homogenous transformation matrix:

$$T_E = R_x(\alpha)R_y(\beta)P_z(r) = \begin{bmatrix} c\beta & 0 & s\beta & rs\beta \\ s\alpha s\beta & c\alpha & s\alpha c\beta & -rs\alpha c\beta \\ -c\alpha s\beta & s\alpha & c\alpha c\beta & rc\alpha c\beta \\ 0 & 0 & 0 & 1 \end{bmatrix}. \quad (9)$$

where $R_k(\theta)$= rotation of θ about k-axis and

$P_z(r)$= translation of r along z-axis.

By comparing the position coordinates in the transformation matrix, the following expression can be obtained:

$$r = \sqrt{x_E^{\,2} + y_E^{\,2} + z_E^{\,2}}, \quad (10)$$

$$\beta = \arcsin\left(\frac{x}{q_8}\right), \quad (11)$$

$$\alpha = \arctan\left(-\frac{y}{z}\right). \quad (12)$$

This coordinates system is essentially a spherical coordinate system and can be related to our generalized joint coordinate system as follows:

$$\begin{pmatrix} q_6 \\ q_7 \\ q_8 \end{pmatrix} = \begin{pmatrix} \alpha \\ -\beta - \frac{\pi}{2} \\ r \end{pmatrix}. \quad (13)$$

Chapter 5 Path Planning and Motion Control

After establishing a mathematically sound kinematics analysis of the design concept, the next phase of the development involves engineering the execution mechanism. This chapter explains the path execution principle and implementation issues. Technical discussion on engineering the mechanical hardware and developing the system software is also presented.

5.1 Multi-axis coordinated joint trajectories

In order to execute remote center of motion, coordination between joints is essential. The design of the proposed manipulator allows natural joint compliant for the constraint at the port opening. Since the design uses the concept of decoupled revolute and prismatic joints, the constraint can be maintained by controlling only the prismatic joints while allowing the revolute joints to move in a compliant manner. Nevertheless, by coordinating at least a pair of revolute-prismatic joint actively, the manipulator can execute RCM base on kinematic constraint. The analytical expression of the trajectories of the kinematics parameters can be derived from the inverse kinematics obtained previously.

From (10), (11), (12) and (13),

$$x = \frac{z}{\cos q_6 \tan q_7} \tag{14}$$

$$y = -z \tan q_6 \tag{15}$$

The time derivative can be expressed as follows

$$\dot{y} = -z\dot{q}_6 \sec^2 q_6 \tag{16}$$

$$\dot{x} = \frac{z(\dot{q}_6 \sin q_6 \tan q_6 - \dot{q}_7 \cos q_6 \sec^2 q_7)}{\cos^2 q_6 \tan^2 q_7} \tag{17}$$

(14), (15), (16) and (17) expressed trajectories of joint 4 and 5 as a function of wrist angular displacement and velocity. Given a constant angular velocity inputs in joint 6 and 7, joint 4 and 5 of Fig. 19 will assume trajectories illustrated in Fig. 20. User can define constant velocity input for one of the rotation-translation pair while varying the other according to the derived trajectories.

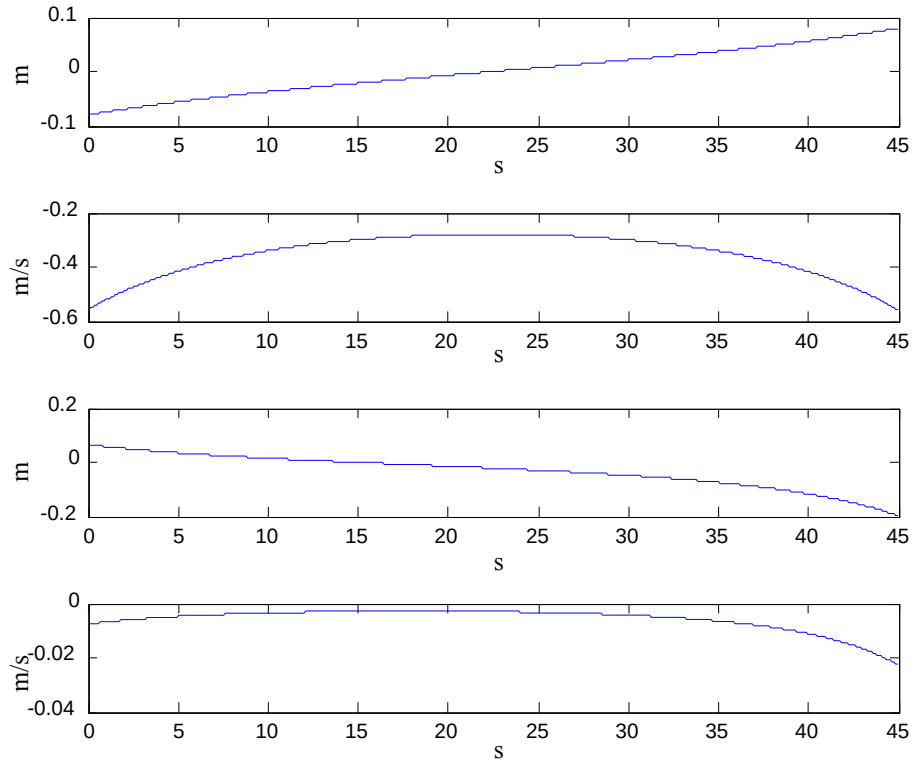

Fig. 20 Trajectory of translational joints required for RCM (a) Displacement profile of joint 4, (b)Velocity profile of joint 4, (c) Displacement profile of joint 5, (d)Velocity profile of joint 5.

For constant angular velocity of 2 degree/s angular position of -30^o to 60^o, in both roll and pitch fashion, the resultant joint trajectories for q_4 and q_5 of Fig. 19 obtained from simulation are as shown in Fig. 21 and Fig. 22. Joint q_6 and q_7 are assumed to have constant velocity and displacement identical to the input simulation signal in Fig. 20.

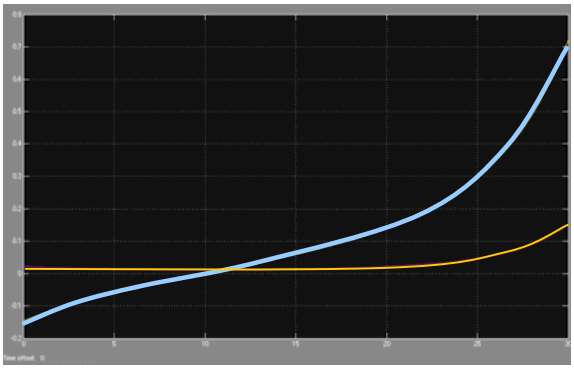

Fig. 21 Trajectory of q_4, thick line represents displacement and thin line represents velocity

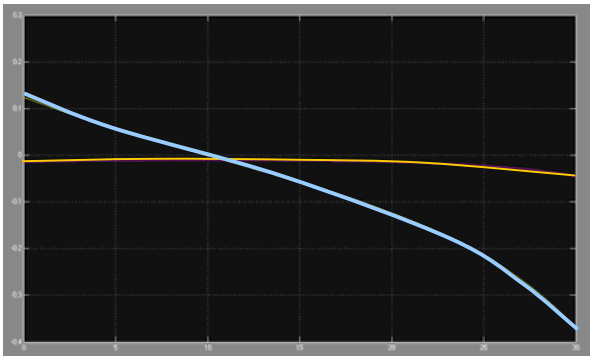

Fig. 22 Trajectories of q_5, Think line represents displacement and thin line represents velocity

The sampling range was intentionally set beyond the joint limits. It can be observed from the graph that the q_4 and q_5 will be infinitely large as the roll and pitch of the surgical tool tends toward 90^o. This reveals a limitation in the system workspace. Singularity occurs when either joint q_6 or q_7 equals 90^o.

5.2 Motion control

5.2.1 Control scheme

The analytical kinematics facilitated the implementation of joint space control scheme. This simplifies algorithmic complexity in the control architecture and favors fast operation for preplanned motion control. Since the implementation of motion control is to facilitate manipulator design and manipulation path plan, the control scheme adopted a model based approach. This work intentionally featured simple motion control solutions relying on knowledge of the derived model instead of sophisticated feedback control architectures. Fig. 23 illustrated the control scheme.

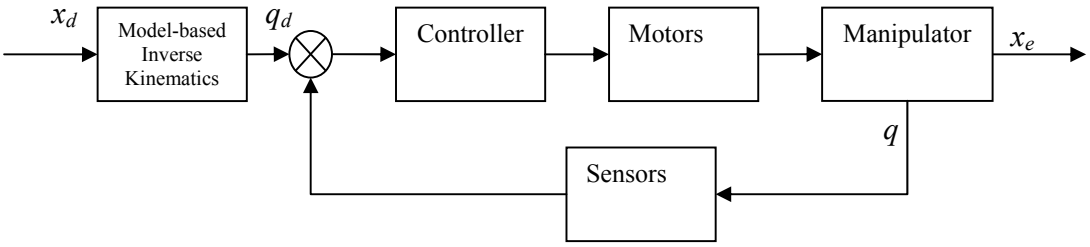

Fig. 23 Motion Control scheme of robotic system

Unlike an operation space control which embedded the inverse kinematics in the feedback control loop, this implementation first solves the inverse kinematics to obtain the desired input in joint space, q_d. It is then controlled based on the actual tracked value of joint output, q. For general manipulator application, this may lead to inaccurate output in the operational space, x_e due to structural uncertainty as the feedback is independent of x_e [67]. However in view of the current task requirement

and system specification with a model based design approach, such an implementation is more appropriate. Operational loads like fiction and inertia are within the specification of the selected stepper motors to avoid slipping. The mechanism was also designed with high precision mechanical component. The subsequent section on hardware selection further explained the hardware implementation aspect of motion control based on the selected control scheme.

5.2.2 Hardware selection and implementation

The motion control hardware involves the range of electronic and mechanical components that drive and maneuver the surgical equipment through the manipulator. These are basically the actuation and sensory elements of the entire mechatronic system.

The sub manipulator is an active P-P-R-R-P manipulator. The prismatic joints were installed with translational stages. Joint 4 and 5 of the serial manipulator are realized using two high precision translational stages of fine screw thread. The constructed planar translational stage has low construction tolerance of $\pm$0.005 mm and resolution of 120 tpi. This enables the mechanism to produce satisfactory results even with simple open loop control mechanism. Joint constraint is hence defined by the travel range of the translational stage with a valued of 100 mm. For the insertion stroke, the maximum travel is 180 mm which is sufficient for laparoscopic surgery.

Similar joint mechanism is used for the manipulation of the projectors as illustrated in Fig. 24. However, the positioning mechanism for the projector system is more

torque demanding because the equipment involved is of larger scale. Larger translation stages are used with ball screw mechanism driver by stepper motors.

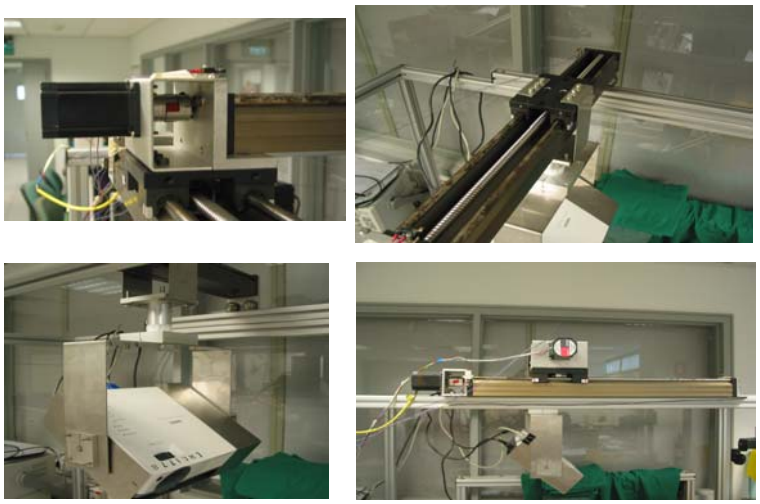

Fig. 24 Joint actuator mechanism for projector manipulation

Finally, motion controls are achieved through software generated pulse train. The pulse train is created in Labview environment and generated as 5 V TTL signal via National Instrument^{TM} M series multifunction DAQ module. This leads to the subsequent discussion on the software programming of the motion control signal.

5.2.3 Software application and operation interface

The software application for motion control was developed using G programming provided by Labview graphical programming environment. The high-level programming environment is excellent for rapid design of the software applications and system integration. In addition, the virtual panel implementation also provides a lean solution to the development of user centric operation interface without going

through costly physical implementation. This helps to foresee issues of usability in the early design phase hence reducing the required design iterations and refinement time or cost within each cycle.

Two modes of operation are developed for robotic control. They include teleoperated and preplanned mode. In teleoperated mode, user controls the motion and the speed of individual joint of the sub manipulator. This mode of operation requires some form of AR or image guidance to be effective. The detailed discussion on the operation workflow is presented in Chapter 6. Preplanned mode on the other hand, is fully automated in execution of large tumor based on preoperative plan. The development is however limited specifically to the execution of overlapping ablation algorithm which will be discussed in Chapter 7.

Fig. 25 depicts a screenshot of the software control interface of teleoperated mode. The user defines the speed at which the selected joint actuator operates and relies on his or her visual judgment and AR guidance to insert the RF probe. Fig. 26 features the preplanned mode which takes in input of ablation coordinates and executed the trajectory automatically. User can specify the operational speed of the wrist joints. The velocity profile of the translational joint will be generated automatically to maintain the RCM.

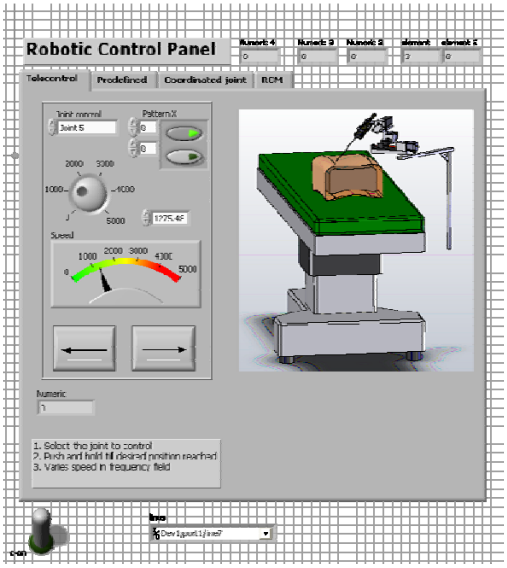

Fig. 25 Teleoperated mode

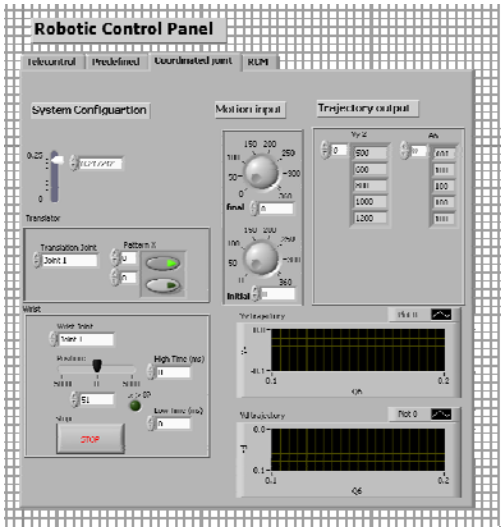

Fig. 26 Preplanned mode

The basic architecture of the control program for preplanned trajectory control involves the application of path planning algorithm, digital pulse train generation and finally acquiring the digital waveform for motor signal. The path planning algorithm is programmed in MathScript code using MathScript Node structure block in Labview.

User defined parameters and system configurations are ‘wired’ to the input of the Node structure and process by the algorithm as shown in Fig. 27. The resultant outputs are sent to the subsequent segment of the trajectory control program.

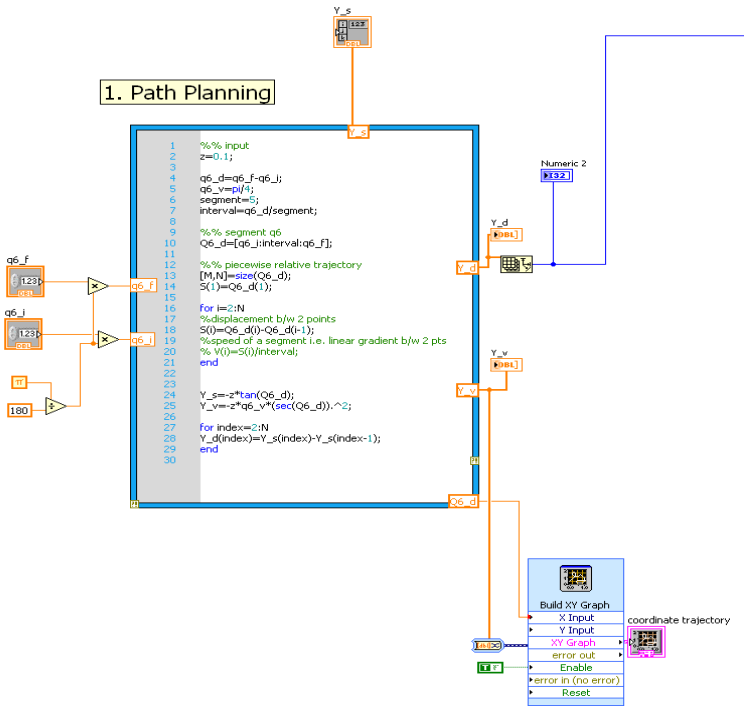

Fig. 27 Implementation of trajectory planning in Labview

Fig. 28 illustrated the program segment for digital signal generation starting from the input of computed trajectories from the path planning algorithm. The on-board counter is deployed for pulse train generation to output the digital signal accordingly.

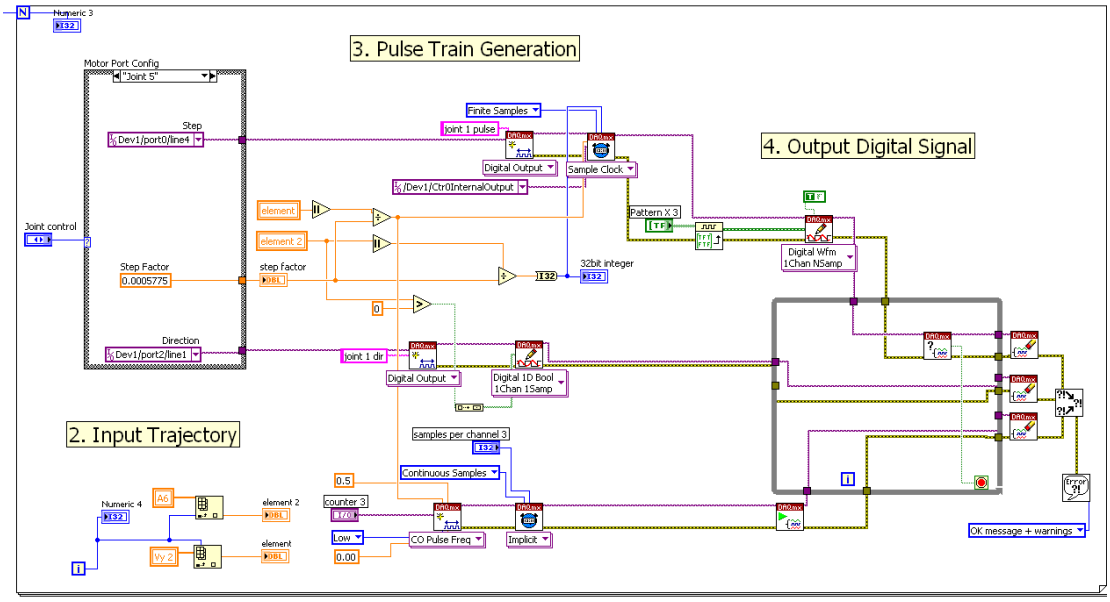

Fig. 28 Software generation of digital signal for desired input trajectory

Chapter 6 Augmented Reality for Intraoperative Guidance

6.1 Principle of direct projected augmented reality

While sophisticated medical imaging modules are available for comprehensive diagnostic and preoperative plans, the effectiveness of surgical treatment lies in the ability to execute the plan with consistency. As such, intraoperative guidance plays an important role in the success of image guided therapies such as ablation of large tumor. Apart from the patient-specific anatomical models facilitated by the primary projector, navigational guidance will be provided by the implementation of the secondary projector. Having a secondary projector to perform intraoperative AR guidance can solve the problem of projection occlusions more effectively without burdening the rest of the system resources. Fig. 29 illustrates the implementation of the two projectors approach for intraoperative visual guidance.

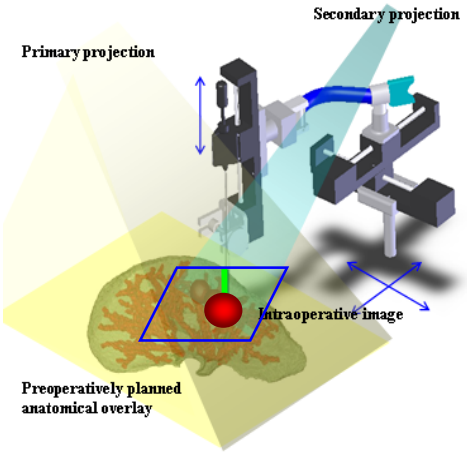

Fig. 29 Illustration of the two projectors approach for projector based AR surgery.

6.2 Intraoperative registration and coordinates transformation

Pre-operation constructed virtual models have to be spatially aligned to correspond to the surgical environment. The process of spatial alignment is referred to as registration. This, in a mathematical definition, is simply to obtain a function that map the corresponding coordinates of one system to another system [1]. For rigid transformation, it can be described by (18):

$$^{B}P_{P} = {}^{B}T_{A}\,{}^{A}P_{P} \tag{18}$$

where

$^{i}T_{j}$= transformation matrix from frame *i* to frame *j*, and

$^{i}P_{j}$= point vector of point *j* wrt frame *i*.

The system is designed to perform image guided surgical plan. Hence, objects identified in medical images must be registered to world coordinates. By doing so, target coordinates in the world reference frame can be obtained and input to the inverse kinematics computational scheme discussed in Chapter 4. For transformation of the image coordinates to world coordinates, a scaling matrix is used based on the intrinsic parameters of the imaging device. Hence the transformation from planar image coordinates to world coordinates is described in (19):

$$^{world}P_{P} = [K]\,^{image}P_{P} \tag{19}$$

where

$^{world}P_{p}$= position vector of point p in world coordinates,

$^{image}P_{p}$= position vector of point p in image coordinates, and

[*K*]= transformation matrix from image to world coordinates.

The z position of the world coordinate can be obtained from the pitch length set for the CT scan. Consequently, the set of relevant 3D world coordinates can be obtained.

6.3 System provision for augmented reality

The developed system uses a combination of passive optical triangulation system and mechanical linkage sensory system is used to establish spatial awareness of the surgical field. Fig. 30 illustrates the installation of tracking system with the robotic manipulator.

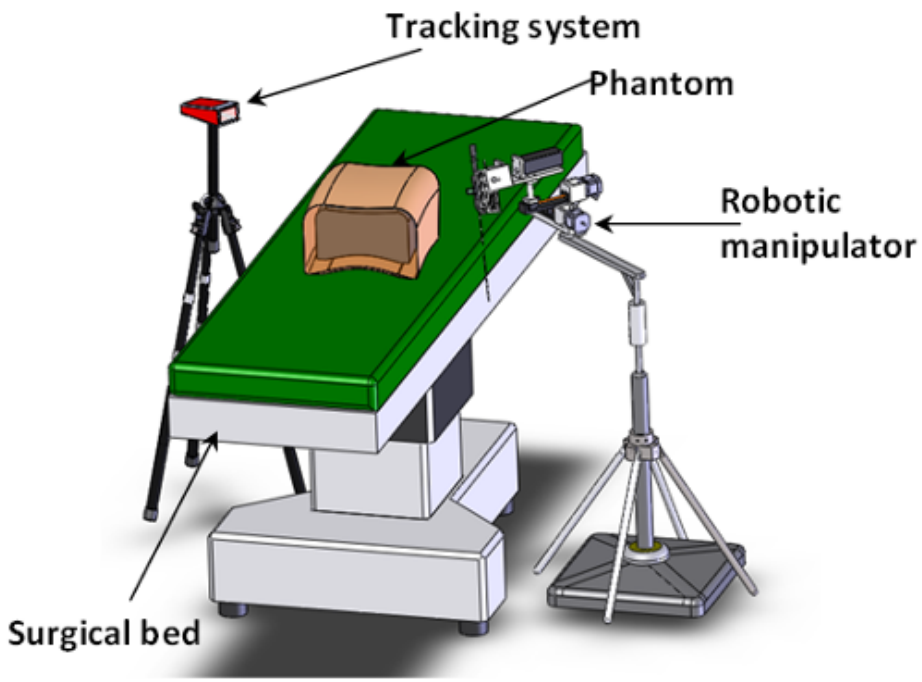

Fig. 30 Robotic installation with tracking system in surgical field

The optical triangulation system registers the coordinates of the points of interest and initializes the frame of reference. This is a neat wireless solution that does not compromise on the real-time performance of robotic execution. Unlike navigation

and tracking, initialization of reference frames during intraoperative registration can be done only once prior to set up. We adopted a generic rigid transformation approach for registration and implemented it with a neat wireless optical triangulation system. This is a non invasive extrinsic approach based on fiducial skin marker. A more comprehensive technical discussion on this topic can be found in [1]. The triangulation system consists of a Leica Disto memo^{TM} laser range finder and an InterSense wireless InertiaCube3^{TM} orientation sensor to provide 3 DOF position tracking. Additional 3 DOF for orientation information for specific component are acquired through a remote set of wireless orientation sensor. Fig. 31 depicts the hardware and software of the registration system.

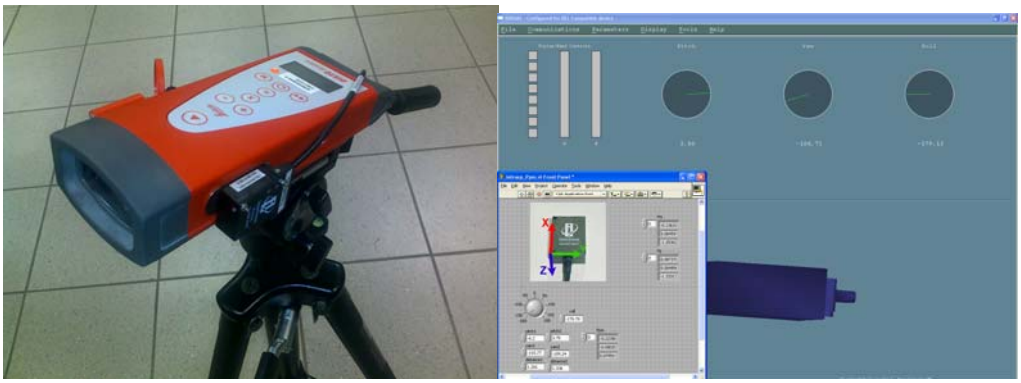

Fig. 31 Coordinates registration system a) hardware setup b) software interface

The robotic attribute of the AR system was exploited for intraoperative navigation and tracking of system components. Automated mechanical translational stages and sensors based articulating linkage are used for navigational tracking of the projector and needle insertion mechanism. Real-time tracking can be effectively implemented by means of mechanical linkage tracking. This provides enormous advantages in

terms of timing performance, system robustness and accuracy compared to a fully camera based or wireless signal approach. Fig. 32 is a scene where the robotic needle insertion device was tested with a laparoscopic camera system.

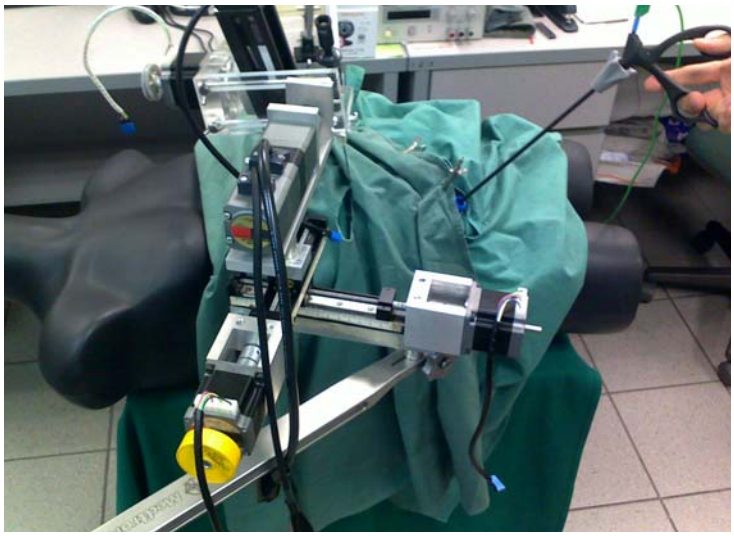

Fig. 32 Robotic needle insertion in laparoscopic procedure on a manikin

6.4 Operation workflow

Fig. 32 illustrates the operation workflow of the AR robotic system. The operation can be divided into five processes.

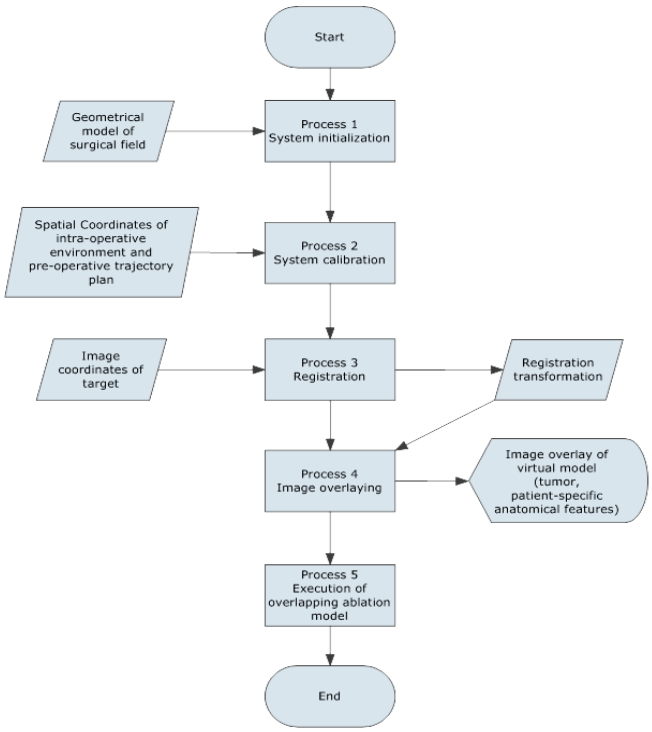

Fig. 33 Operation process flow of the AR robotic system

Process 1: System initialization

A global frame of reference based on the geometrical model of the surgical field will be assigned. The aim is to establish spatial reference to the surgical system and enable registration of the pre-operative planning to the intraoperative environment subsequently.

Process 2: System calibration

The robotic needle insertion manipulator is calibrated to the projection system. This includes the derivation of a geometrical transformation describing the spatial relationship between the two sub-systems. This can be done by processing the kinematic models discussed previously with geometric parameters. The transformation matrix will subsequently enable the expression of kinematics of the components to be referenced in the same domain.

Process 3: Registration

Virtual models need to be reference with respect to real world coordinates. This can be done by a few developed techniques depending on the specific system requirements [68].

Process 4: Image overlaying

Application of the registration transformation obtained from process 3 to manipulate the image projection such that the targets corresponds to the tumors or the image data is matched accurately to its corresponding features. The image coordinate of the targets should be derived from pre-operative computer processed imaging and surgical plan. By processing the image with prewarp transformation function, the corresponding feature points can be aligned onto the projection plane to provide a direct projected visualization to the surgeon.

Process 5: Execution of overlapping ablation model

Multiple needle insertion and deployment of needle will be done under intraoperative guidance of the AR projection. This can be carried out in three classes of modes. First, the surgeon can choose to tele-operate the manipulator with the visual augmentation. He can also collaboratively operate the robotic assistive device by dedicating certain

tasks like spatial positioning or depth insertion. Lastly, he has the option to automate the entire overlapping ablation specifying only the incision site based on the AR guidance.

Chapter 7 Robotic Overlapping Ablation for Large Tumor

This chapter explains the workflow and principle behind the application of the robotic system in an interventional technique for large tumor treatment known as overlapping ablation. It involves the interpretation of preoperative diagnostic information, overlapping ablation plan, intraoperative registration and coordinates transformation, and robotic execution of the ablation plan.

7.1 Preoperative diagnosis

Surgical treatment of liver tumor typically starts with the acquisition of relevant pathological information and patient specific anatomical knowledge through diagnostic imaging modalities. Specialized image processing software is then used to carry out segmentation. A virtual model containing information, relative spatial coordinates of the tumor and other vital anatomical structures can be constructed by volume rendering method.

7.2 Overlapping ablation plan

An automatic algorithm for the generation of the ablation plan is developed. It adopted a “voxel growing” algorithm to automatically produce the ablation points according to the tumor’s irregular profile in 3D. To further reduce number of required ablation and minimize burning of healthy tissue, the “grown region” is aligned to best fit the geometry of the target region. Our method involves the construction of spherical elements defined by inscribed cubes. Each sphere

represents the ablation area, and its inscribed cube represents a voxel element. Voxel elements will fill the tumor and cover the entire volume of the tumor. In order to best fit the entire ablation area to comply with the contour of the tumor, the voxel elements are propagated layer by layer within the tumor according to its local surface. The model coordinate is set up the same way as the surface coordinate. The input for the ablation model is the surface data of the tumor, which is acquired from CT scan in advance. The algorithm is presented as follows.

Step 1: Determine the size of a voxel element

First we need to specify the size of a voxel element. This is determined by defining the dimension of a single ablation sphere. For a sphere of diameter *D*, the length of its inscribed cube is *d* as represented in Fig. 34.

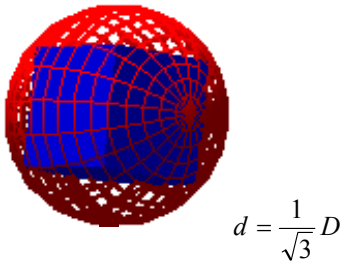

Fig. 34. Element of the ablation model

The maximum ablation size is used to minimize required number of ablations. For most RF device, this value is 50 mm [9].

Step 2: Compute required layer along z-axis

A 3D image coordinate system is established based on the series of CT scan.

Assume the z coordinates of the surface data are *s{ s(1, z), s(2, z), …… s(i, z)……,s(n-1, z), s(n, z)}* where *i* is the i^{th} coordinate of the surface data which is

expressed in 3D coordinate, and *z* is the *z* coordinate. We can compute the largest *z* and the smallest *z* among the surface data through the iteration from 1 to *n*:

```
for i=1:n

if s(i-1, z)< s(i, z) then
        X=s(i, x)
        Y=s(i, y)
        Z_largest =s(i, z)

else
        X=s(i-1, x)
        Y=s(i-1, y)
        Z_largest =s(i-1,z)
```

where *s(i, x)* and *s(i, y)* are the i^{th} *x* coordinate and *y* coordinate of the surface data, *X, Y* are the *x* coordinate and *y* coordinate with largest *z* coordinate. The resultant *z* coordinates for the two extreme can be represented mathematically by

$$Z_{\text{largest}} = \max\left(s(i,z) \mid 1 \le i \le n\right) \text{ and}$$

$$Z_{\text{smallest}} = \min\left(s(i,z) \mid 1 \le i \le n\right). \tag{20}$$

Since each layer is one voxel thick, the height of each layer *i*s d.

Number of layers, L can be computed by

$$L = \text{ceil}\left((Z_{\text{largest}} - Z_{\text{smallest}})/d\right). \tag{21}$$

Function ceil returns the largest integer for the number of the layers.

Step 3: Coordinates assignment of each layer

The step addresses two issues in the arrangement of voxel. First, the element needs to be in a proper location to ensure the coverage of tumor with different contour while minimizing on the required ablation volume. Second, the algorithm needs to

be able to adapt to various shape of the tumor. The fitting of tumor's shape automatically for such cases is a challenging task.

The distribution of the element voxel model is adjusted along z axis and propagated layer by layer to conform to the shape of the tumor. The center point of the tumor along z axis, Z_{origin} can be calculated by (22).

$$Z_{\text{origin}} = \frac{1}{2}\left(Z_{\text{largest}} + Z_{\text{smallest}}\right) \tag{22}$$

Equation (23) establishes the z coordinates of the first layer.

For i^{th} layer,

$$Z_i = Z_{\text{origin}} - (i \times d) \tag{23}$$

In this approach, specific tumor segment is more appropriately bounded within the voxelized region along the z direction. This alignment of the voxelized region which better fits the tumor segment actually minimizes the number of ablation sphere required. As a result of the geometric conformity, less healthy tissue will be affected by the thermal injury. This assignment scheme is further extended to *x*-axis and *y*-axis direction.

Step 4: Intra-layer propagation

Similar boundaries establishment is applied along the *x*-axis and eventually the *y*-axis. This is done in a layer by layer scheme as indexed in Step 2. With the best fitting boundaries defined, the coordinates continue to propagate within that specific layer in *x*-axis direction until the *x* and *z* coordinates are computed.

Similarly, the *y* coordinates are assigned with the same approach along the *y*-axis until eventually the *x,y* and *z* coordinates of the specific layer are fully defined.

Step5: Iteration for subsequent layer

The above steps will iterate for subsequent layers until sufficient ablation coverage for the entire tumor is generated by these voxels. Eventually, spherical elements will circumscribe over each voxel element to represent the ablation region. Fig. 35 illustrated the process of overlapping ablation planning.

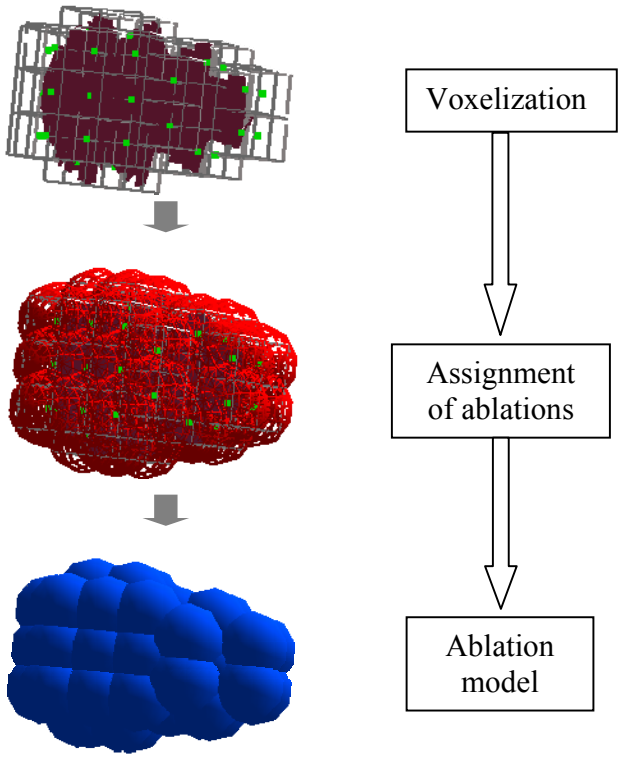

Fig. 35 **Construction of optimal ablation model; brown figure: virtual construction of tumor, Green dots: designated location of needle tips, red wireframe: predicted ablation region, blue: resultant necrosis region**

This planning algorithm is based on clinically relevant optimizing conditions and well established clinical practices. We adapt our planning algorithm based on the

cylindrical model discussed in [8]. As such our model adopts uniform spherical ablation zone with similar linear pattern in a three dimensional space. However, the configurations of these linear rows are "packed" in an optimal fashion to conform to the irregularity of the tumor geometry. This will reduce the destruction of healthy tissue which work towards the same objective defined by Baegert *et al* [69]. However the upmost priority of our treatment plan is to ensure complete ablation of the entire tumor because leaving any tumor cell untreated can lead to recurrence and further spreading of the tumor. Hence, our planning strategy skewed conservatively towards complete ablation coverage of target rather than attempting optimal control of ablation geometry. In essence, our method aims to minimize number of needle insertions while providing sufficient ablation coverage of the entire targeted region without causing unnecessary thermal injury to healthy tissue.

Despite being in agreement with many of the criteria defined in existing literature [10, 46, 69], we recognize that there are other clinical considerations and case-specific prioritization of criteria. There is generally no one-size-fits-all solution for the best ablation model. However, the systematic nature of our approach made the method executable with simple manipulator trajectories yet highly adaptive to various clinical cases. For instance, surgeon might consider prioritizing conservation of hepatic reserve over operation duration and minimizing needle punctures. In such situation, the outer most voxel elements exposed to healthy tissue can be further subdivided to refine the contour conformity of the model ablation region. This may be done at the expense of more needle punctures and longer operation duration.

7.3 Coordinate transformations and robotic execution

A computation scheme to obtain the relative transformation matrix from the trocar to the target point is required as the input to the previously discussed inverse kinematics computational scheme. This is illustrated as follows.

Step 1: Obtain transformation of target point with respect to fiducial marker frame

$$^{M}T_{T} = [K]^{M'}T_{T'} \tag{24}$$

M and *M'* denote frame assigned to fiducial marker in world coordinates and image coordinates respectively. *T* and *T'* denote frame assigned to target point in world and image coordinates.

Step 2: Obtain transformation of incision port with respect to fiducial marker frame

The principle is to acquire a geometrical relationship of the incision port and the fiducial marker.

$$^{P}T_{M} = ^{P}T_{G}\,^{G}T_{M} \tag{25}$$

P denotes frame assigned to incision port, *M* denotes frame assigned to fiducial marker and *G* denotes a chosen global frame.

Step 3: Obtain transformation target point with respect to incision port

$$^{P}T_{T} = ^{P}T_{M}\,^{M}T_{T} \tag{26}$$

The derived overlapping ablation plan is finally achieved through robotic execution. This is done by a model based preplanned trajectories control. The target points are obtained from the overlapping ablation plan. This is the final stage where the entire preplanning procedures discussed previously are translated to intraoperative execution of joint trajectories. The surgeon will activate the needle

insertion trajectory sequentially while the RF generator regulated the ablation region. Once the each ablation is complete, the surgeon will activate the subsequent insertion trajectory. Eventually the set of preplanned trajectories will create an overlapping ablation zone that encompasses the entire tumor.

Chapter 8 Result and Discussion

8.1 Design evaluation on workspace and dexterity

Workspace is an important criterion for manipulator design. The workspace of the manipulator has to fulfill the kinematic requirement of the overlapping ablation application established previously. The workspace of the manipulator system was analyzed using volumetric approach [61]. Piecewise calculus is used to generate the workspace as shown in a screenshot of Fig. 36.

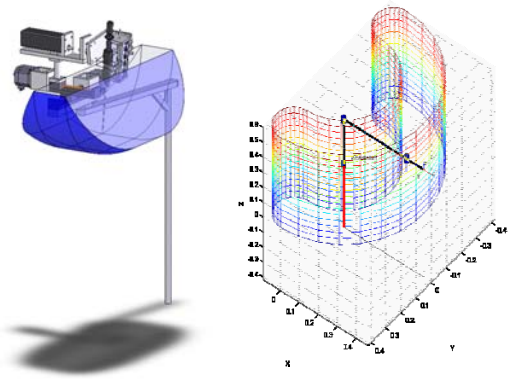

Fig. 36 Workspace of manipulator Left: sub manipulator and Right main manipulator

From the calculated workspace volume, the structural length index , Q_L [70] can be obtained. The index explains the workspace envelop of the manipulator design. The structural length index of the prototypical manipulator has a value of 1.44. This is reasonably close to an optimal articulating arm (Q_L≈0.62) and much better than a Cartesian manipulator (Q_L=3).

The sub manipulator design principle was based on geometric optimization mentioned previously. When the needle tip is drawn to the intersection of the

orthogonal revolute joint it can be orientated in all direction. This is known as the dexterous point [49]. The regional structure includes the prismatic joints which position the needle tip in the x-y plane. The surface encompasses all the dexterous point and determined by the joint limits of joint 4 and 5 as illustrated in Fig. 37.

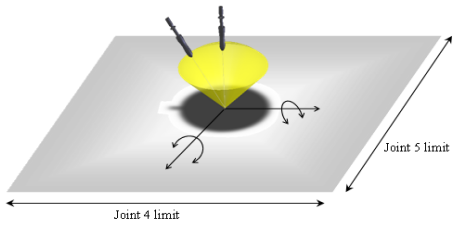

Fig. 37 Surface containing dexterous points for a given elevation plane

The dexterous workspace of the mechanism can therefore be represented by the swept volume of the passive manipulator. Fig. 38 feature the dexterous workspace produced by CAD software. Its geometry is determined by the reachable workspace of the passive manipulator.

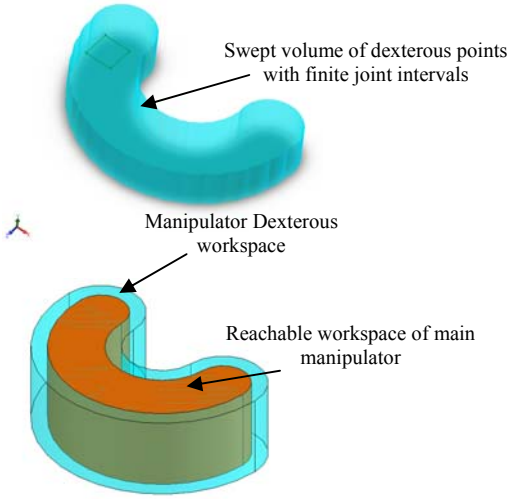

Fig. 38 Dexterous workspaces

The concept of manipulability [71-73] is being used for dexterity measures. Manipulability, w can be represented by (27). A high index implies high dexterity.

$$w = \sqrt{\det(JJ^T)} \tag{27}$$

where J is the Jacobian matrix.

The manipulator is able to achieve a mean manipulability of 0.98 within its joint limit. This value is promising compared to the value of 0.128 for Zeus system. Zeus robotic surgical system though no longer commercially available, continues to be a common standard of comparison for researches related to minimally invasive surgical robots [58, 74].

8.2 Computation Time

Simulation based evaluation is an essential aspect of assessment prior to the materialization of a system. We construct a virtual model of our manipulator using Robotics toolbox [48] equipped in Matlab™ and measure computation time of the inverse kinematics scheme, which is important for the performance of overlapping ablation. The mean computation time of the inverse kinematics scheme is approximately 0.365 ms on a personal computer with Pentium D, 3.0GHz and 2GB memory, which can fulfill the real-time requirement. This is based on calculation with 1000 randomly generated target points.

On the other hand, to assess the speed performance of the ablation planning algorithm, a phantom tumor with 256 surface points coordinate were constructed. The time to compute and establish the ablation plan is on average 5.5 s. This result is

promising compared to existing optimization work which requires a few minutes of converge time for typical large tumor [46].

8.3 Experiments

8.3.1 Tracking accuracy and needle path consistency

The intraoperative tracking system is put to test for a specific predefined motion trajectory of our developed robotic end effector needle insertion device [36]. Fig. 39 shows the differences between the track position coordinates and the actual path taken. The mean error of our current system is 0.8 pixel by 1.7 pixel. Depending on the specification of the camera and the operating distance of the image plane and object plane the error in the world coordinate system can be different. In a typical operation range, the planar tracking error approximately translated to an error of 0.8 mm by 1.7 mm for a camera system with resolution of 640 by 480 pixels.

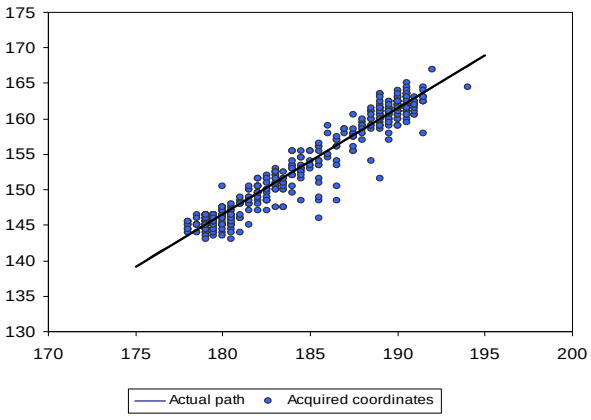

Fig. 39 Vision based tracking accuracy

This deviation is insignificant considering the safety margin of 10 mm adopted in clinical practice [9].

8.3.2 Ex-vivo experiment

The feasibility of our developed prototypical system is validated through ex-vivo tests on porcine liver. Radiofrequency ablation is carried out with the RITA System using our developed robotic prototype. The RITA system comprises mainly of the Model 1500X Electrosurgical RF generator and a 14G RITA Starburst Electrosurgical Device. Fig. 40 shows the setup of the robotic system in an advance training surgical theater. Fig. 41 zooms in on the sub-manipulator system during experimental operation and the effect of ablation on a porcine liver.

In the first experiment a virtual tumor model is constructed. The proposed planning algorithm is subsequently applied to generate an overlapping ablation model. Finally, the robotic system executes the required path to create a necrosis region defined by the ablation model on ex-vivo porcine liver.

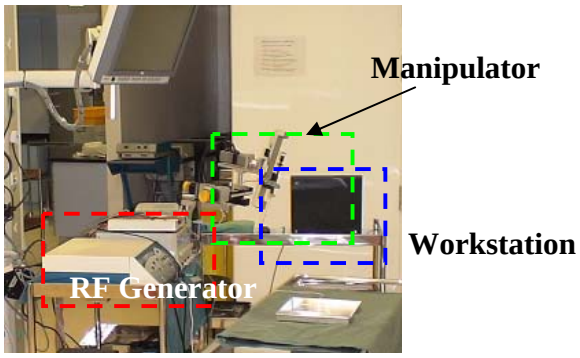

Fig. 40 Setup of robotic system in surgical training facility

Fig. 41 Sub manipulator for overlapping ablation experiment

Fig. 42 shows the measurements of two overlapping necrosis regions. This region of interest represented a 17 mm by 8.5 mm by 8.5 mm voxelized target to be covered by two spheres. Each sphere is 15 mm as shown Fig. 42(A). The intended ablation for this region should span over a distance of 23.5mm instead of the 25.27 mm shown in Fig. 42(B). As such the error in position is approximate 1.77mm.

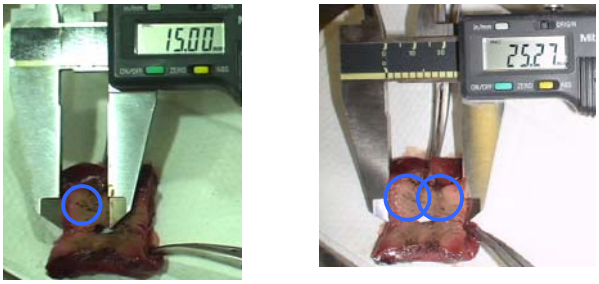

Fig. 42 Tissue necrosis created by (A) single RFA and (B) overlapping RFA

In the second ex-vivo experiment, a phantom tumor with contrast medium is injected into the liver. The liver is subsequently sent for CT scanning and its image data used for 3D reconstruction. The proposed planning algorithm is applied to generate an overlapping ablation model. Finally, the robotic system executes the required path to create a necrosis region defined by the ablation model on ex-vivo porcine liver.

Fig. 43 shows the ablation of the phantom tumors. The average deviation in concentricity between the ablated zone and the phantom tumor is 1.5 mm. This is done by the measurement of the difference in ablation radius and tumor radius.

Fig. 43. Single ablation of phantom tumor

Accuracy of needle insertion is usually compromised by uncertainties like tissue deformation, needle deflection, motion of subject due to respiration or heartbeats, and registration misalignment. Of all these, modeling deformation in organ is the most challenging task. This is due to the complexity associated with the modeling of soft tissue, organ geometry and boundary constraints. Soft tissue is usually inhomogenous, nonlinear, anisotropic, and viscoelastic [75]. The patient specific nature of soft tissue behavior also renders generalized soft tissue properties inaccurate for tissue modeling. Moreover it was showed that organ geometry and boundary constraint are the dominant factors for deformation [76]. This is a topic of great research interest. It is however, independent to our design centric objective as the predictive model can be easily integrated into the ablation planning algorithm once a reliable organ deformation model is available.

The slight needle misplacement reported could be a result of tissue deformation. However, this result can be argued to be acceptable as it falls within the clinically recommended 10 mm safety margin. This sufficiently supports the feasibility and suggests promising potential in the proposed system. There is no doubt that modeling organ deformation and needle-tissue interaction will be one of our further directions to perfect the effectiveness of the system.

Chapter 9 Recommendation and Conclusion

An augmented reality robotics system consisting of a robotic projection system and a novel manipulator design for needle insertion was developed. The projection system was designed to overlay anatomical information aiding surgeon in decision like incision port placement and the navigation of surgical tools while the needle insertion manipulator perform large tumor treatment through the execution of multiple needle insertion. This module is capable of executing an automatic ablation planning algorithm. Hence, it addresses the clinical issue of manual treatment for large tumor using RF ablation.

To date, two animal experiments (IACUC Protocol Number 096/08; T18/08) have been performed with the robotic needle insertion manipulator. These studies are conducted in collaboration with the surgeons and radiologists in National University Hospital, Singapore. Data supported the feasibility of the manipulator design which yields promising results in terms of accuracy and precision. The robustness of the system against intraoperative uncertainties should however be further improved. Such uncertainties have been discussed in the previous section. The issue of compensation for tissue deformation should be addressed in future studies. Soft tissue deformation is more than the mere modeling of organ geometry and constitutive behavior of the soft tissue. Misra *et al* [76] has shown the importance of boundary constraints on tissue deformation in addition to organ geometry. Traditional simulation method produces nodal displacement of 14 times larger than actual anatomical model. Current knowledge in organ deformation is helpless against the complex uncertainties

of organ geometry and boundary constraint. The large deviation in the prediction can lead to worse misplacement of needle than an uncorrected trajectory. Existing deformation models may have reasonable realism in simulation training model but could introduce more uncertainties to a complex surgical planning model. This subject requires extensive theoretical and experimental studies and is definitely an interesting topic for future exploration.

While the needle insertion manipulator has matured to be functionally capable, it can be further perfected with refinement in the execution algorithm, design implementation and overall robustness. The study of issues like obstacle avoidance and dexterity constraint in real surgical setting is significant to further demonstrate the efficacy of the system. The established framework will act as a platform for continual experimentation on intelligent algorithms for obstacle avoidance and dexterity constraint detection in actual surgical environment. Streamlining of design towards an acceptable standard for clinical trial can also be conducted base on current infrastructure. The augmented reality robotic system will eventually combine with technologies and medical innovations [24, 77] being developed in parallel. Seamless integration of the system into an augmented reality based surgical system will provide surgeons with intraoperative feedback and realistic visual guidance.

References

[1] R. H. Taylor, P. Kazanzides, and F. David Dagan, "Medical Robotics and Computer-Integrated Interventional Medicine," in *Biomedical Information Technology* Burlington: Academic Press, 2008, pp. 393-416.

[2] B. Nordlinger, M. Guiguet, J. C. Vaillant, P. Balladur, K. Boudjema, P. Bachellier, and D. Jaeck, "Surgical resection of colorectal carcinoma metastases to the liver. A prognostic scoring system to improve case selection, based on 1568 patients. Association Francaise de Chirurgie," *Cancer,* vol. 77, pp. 1254-62, Apr 1 1996.

[3] "Primary liver cancer in Japan. Clinicopathologic features and results of surgical treatment. Liver Cancer Study Group of Japan," *Ann Surg,* vol. 211, pp. 277-87, Mar 1990.

[4] S. Benoist and B. Nordlinger, "Radiofrequency ablation in liver tumours," *Ann Oncol,* vol. 15 Suppl 4, pp. iv313-7, 2004.

[5] W. Y. Lau, T. W. Leung, S. C. Yu, and S. K. Ho, "Percutaneous local ablative therapy for hepatocellular carcinoma: a review and look into the future," *Ann Surg,* vol. 237, pp. 171-9, Feb 2003.

[6] J. P. McGhana and G. D. Dodd, 3rd, "Radiofrequency ablation of the liver: current status," *AJR Am J Roentgenol,* vol. 176, pp. 3-16, Jan 2001.

[7] T. F. Wood, D. M. Rose, M. Chung, D. P. Allegra, L. J. Foshag, and A. J. Bilchik, "Radiofrequency ablation of 231 unresectable hepatic tumors:

indications, limitations, and complications," *Ann Surg Oncol,* vol. 7, pp. 593-600, Sep 2000.

[8] G. D. Dodd, 3rd, M. S. Frank, M. Aribandi, S. Chopra, and K. N. Chintapalli, "Radiofrequency thermal ablation: computer analysis of the size of the thermal injury created by overlapping ablations," *AJR Am J Roentgenol,* vol. 177, pp. 777-82, Oct 2001.

[9] M. H. Chen, W. Yang, K. Yan, M. W. Zou, L. Solbiati, J. B. Liu, and Y. Dai, "Large liver tumors: protocol for radiofrequency ablation and its clinical application in 110 patients--mathematic model, overlapping mode, and electrode placement process," *Radiology,* vol. 232, pp. 260-71, Jul 2004.

[10] C. Baegert, C. Villard, P. Schreck, L. Soler, and A. Gangi, "Trajectory optimization for the planning of percutaneous radiofrequency ablation of hepatic tumors," *Comput Aided Surg,* vol. 12, pp. 82-90, Mar 2007.

[11] V. Scheinman and J. M. McCarthy, "Mechanisms and Actuation," in *Springer Handbook of Robotics*, 2008, pp. 67-86.

[12] J. Angeles and F. C. Park, "Performance Evaluation and Design Criteria," in *Springer Handbook of Robotics*, 2008, pp. 229-244.

[13] V. Miomir, P. Veljko, I. Kenji, and T. Masaharu, *The mechanical systems design handbook : modeling, measurement, and control*. Boca Raton, FL :: CRC Press, 2002.

[14] N. Koizumi, S. Warisawa, M. Mitsuishi, and H. Hashizume, "Continuous path controller of slave manipulator in remote ultrasound diagnostic system," in

Robotics and Automation, 2002. Proceedings. ICRA '02. IEEE International Conference on, 2002, pp. 3368-3373 vol.4.

[15] D. Qinjun, H. Qiang, T. Libo, and L. Chuncheng, "Mechanical Design and Control System of a Minimally Invasive Surgical Robot System," in *Mechatronics and Automation, Proceedings of the 2006 IEEE International Conference on*, 2006, pp. 1120-1125.

[16] M. Jakopec, S. J. Harris, F. Rodriguez y Baena, P. Gomes, J. Cobb, and B. L. Davies, "The first clinical application of a "hands-on" robotic knee surgery system," *Comput Aided Surg,* vol. 6, pp. 329-39, 2001.

[17] *Fundamentals of laparoscopic surgery* vol. 881098. New York: : Churchill Livingstone, 1995.

[18] M. C. Cavusoglu, F. Tendick, M. Cohn, and S. S. Sastry, "A laparoscopic telesurgical workstation," *Robotics and Automation, IEEE Transactions on,* vol. 15, pp. 728-739, 1999.

[19] "The 3rd Asian Conference on Computer Aided Surgery (ACCAS) by SSAGSg-Society of Simulation and Gaming of Singapore," Singapore: : Society of Simulation and Gaming of Singapore, 2007, pp. 1 CD-ROM : col. ; 4 3/4 in.

[20] G. Fichtinger, A. Deguet, K. Masamune, E. Balogh, G. S. Fischer, H. Mathieu, R. H. Taylor, S. J. Zinreich, and L. M. Fayad, "Image overlay guidance for needle insertion in CT scanner," *Biomedical Engineering, IEEE Transactions on,* vol. 52, pp. 1415-1424, 2005.

[21] J. Hong, T. Dohi, M. Hashizume, K. Konishi, and N. Hata, "An ultrasound-driven needle-insertion robot for percutaneous cholecystostomy," *Physics in Medicine and Biology,* vol. 49, 2004-02-07 2004.

[22] D. Qinjun, H. Qiang, L. Chuncheng, and Z. Weimin, "Research on Control System of Radio Frequency Ablation Surgical Robot," in *Robotics and Biomimetics, 2006. ROBIO '06. IEEE International Conference on*, 2006, pp. 1287-1292.

[23] D. Qinjun and Z. Xueyi, "Research on robotic technologies for ultrasound guided radio frequency ablation surgery," in *Industrial Technology, 2008. ICIT 2008. IEEE International Conference on*, 2008, pp. 1-6.

[24] F. Leong, L. Yang, S. Chang, A. Poo, I. Sakuma, and C.-K. Chui, "A Precise Robotic Ablation and Division Mechanism for Liver Resection," in *Medical Imaging and Augmented Reality*, 2008, pp. 320-328.

[25] J. Marescaux, L. Soler, and F. Rubino, "Augmented Reality for Surgery and Interventional Therapy," *Operative Techniques in General Surgery,* vol. 7, pp. 182-187, 2005.

[26] C. Nikou, A. M. Digioia Iii, M. Blackwell, B. Jaramaz, and T. Kanade, "Augmented reality imaging technology for orthopaedic surgery," *Operative Techniques in Orthopaedics,* vol. 10, pp. 82-86, 2000.

[27] M. Blackwell, C. Nikou, A. M. DiGioia, and T. Kanade, "An Image Overlay system for medical data visualization," *Medical Image Analysis,* vol. 4, pp. 67-72, 2000.

[28] D. A. Wang, F. Bello, and A. Darzi, "Augmented reality provision in robotically assisted minimally invasive surgery," *International Congress Series,* vol. 1268, pp. 527-532, 2004.

[29] N. Abolhassani, R. Patel, and M. Moallem, "Experimental study of robotic needle insertion in soft tissue," *International Congress Series,* vol. 1268, pp. 797-802, 2004.

[30] M.-A. Janvier, L.-G. Durand, M.-H. R. Cardinal, I. Renaud, B. Chayer, P. Bigras, J. de Guise, G. Soulez, and G. Cloutier, "Performance evaluation of a medical robotic 3D-ultrasound imaging system," *Medical Image Analysis,* vol. 12, pp. 275-290, 2008.

[31] I. Balasingham, E. Samset, A. Hansen, and L. Aurdal, "An interactive augmented reality 3D visualization system for destroying liver tumor using cryoablation," *International Congress Series,* vol. 1256, pp. 690-695, 2003.

[32] N. D. Glossop and Z. Wang, "Laser projection augmented reality system for computer-assisted surgery," *International Congress Series,* vol. 1256, pp. 65-71, 2003.

[33] R. Krempien, H. Hoppe, L. Kahrs, S. Daeuber, O. Schorr, G. Eggers, M. Bischof, M. W. Munter, J. Debus, and W. Harms, "Projector-Based Augmented Reality for Intuitive Intraoperative Guidance in Image-Guided 3D Interstitial Brachytherapy," *International Journal of Radiation Oncology Biology Physics,* vol. 70, pp. 944-952, 2008.

[34] S. A. Nicolau, X. Pennec, L. Soler, X. Buy, A. Gangi, N. Ayache, and J. Marescaux, "An augmented reality system for liver thermal ablation: Design

and evaluation on clinical cases," *Medical Image Analysis,* vol. 13, pp. 494-506, 2009.

[35] J. Traub, M. Feuerstein, M. Bauer, E. U. Schirmbeck, H. Najafi, R. Bauernschmitt, and G. Klinker, "Augmented reality for port placement and navigation in robotically assisted minimally invasive cardiovascular surgery," *International Congress Series,* vol. 1268, pp. 735-740, 2004.

[36] L. Yang, C.-K. Chui, and S. Chang, "Design and Development of an Augmented Reality Robotic System for Large Tumor Ablation," *International Journal of Virtual Reality,* vol. 8, pp. 27-35, 2009.

[37] S. Byung-Kuk, L. Moon-Hyun, P. Hanhoon, P. Jong-Il, and K. Young Soo, "Direct-Projected AR Based Interactive User Interface for Medical Surgery," in *Artificial Reality and Telexistence, 17th International Conference on*, 2007, pp. 105-112.

[38] L.-M. Su, B. P. Vagvolgyi, R. Agarwal, C. E. Reiley, R. H. Taylor, and G. D. Hager, "Augmented Reality During Robot-assisted Laparoscopic Partial Nephrectomy: Toward Real-Time 3D-CT to Stereoscopic Video Registration," *Urology,* vol. In Press, Corrected Proof, 2009.

[39] H. Park, M.-H. Lee, S.-J. Kim, and J.-I. Park, "Surface-Independent Direct-Projected Augmented Reality," in *Computer Vision – ACCV 2006*, 2006, pp. 892-901.

[40] C. Bichlmeier, S. Holdstock, S. M. Heining, S. Weidert, E. Euler, O. Kutter, and N. Navab, "Contextual in-situ visualization for port placement in keyhole surgery: Evaluation of three target applications by two surgeons and eighteen

medical trainees," in *Proceedings of the 2009 8th IEEE International Symposium on Mixed and Augmented Reality*: IEEE Computer Society, 2009.

[41] M. Figl, D. Rueckert, D. Hawkes, R. Casula, M. Hu, O. Pedro, D. P. Zhang, G. Penney, F. Bello, and P. Edwards, "Image guidance for robotic minimally invasive coronary artery bypass," *Computerized Medical Imaging and Graphics,* vol. 34, pp. 61-68, 2010.

[42] E. McGarrity and M. Tuceryan, "A method for calibrating see-through head-mounted displays for AR," in *Augmented Reality, 1999. (IWAR '99) Proceedings. 2nd IEEE and ACM International Workshop on*, 1999, pp. 75-84.

[43] H. Park and J.-I. Park, "Modern Approaches to Direct-Projected Augmented Reality: A Review," in *4th international symposium on ubiquitous VR*, 2006, pp. 892-901.

[44] S.-L. Lee, M. Lerotic, V. Vitiello, S. Giannarou, K.-W. Kwok, M. Visentini-Scarzanella, and G.-Z. Yang, "From medical images to minimally invasive intervention: Computer assistance for robotic surgery," *Computerized Medical Imaging and Graphics,* vol. 34, pp. 33-45, 2010.

[45] S. P. DiMaio and S. E. Salcudean, "Interactive simulation of needle insertion models," *Biomedical Engineering, IEEE Transactions on,* vol. 52, pp. 1167-1179, 2005.

[46] C. Villard, L. Soler, and A. Gangi, "Radiofrequency ablation of hepatic tumors: simulation, planning, and contribution of virtual reality and haptics," *Computer Methods in Biomechanics and Biomedical Engineering,* vol. 8, pp. 215 - 227, 2005.

[47] B. Davies, "A review of robotics in surgery," *Proc Inst Mech Eng [H],* vol. 214, pp. 129-40, 2000.

[48] P. I. Corke, "A robotics toolbox for MATLAB," *Robotics & Automation Magazine, IEEE,* vol. 3, pp. 24-32, 1996.

[49] J. J. Craig, *Introduction to Robotics Mechanics and Control* Prentice Hall, 2005.

[50] C.-H. Kuo and J. S. Dai, "Robotics for Minimally Invasive Surgery: A Historical Review from the Perspective of Kinematics," in *International Symposium on History of Machines and Mechanisms*, 2009, pp. 337-354.

[51] R. H. Taylor and D. Stoianovici, "Medical robotics in computer-integrated surgery," *Robotics and Automation, IEEE Transactions on,* vol. 19, pp. 765-781, 2003.

[52] M. J. H. Lum, J. Rosen, M. N. Sinanan, and B. Hannaford, "Optimization of a spherical mechanism for a minimally invasive surgical robot: theoretical and experimental approaches," *Biomedical Engineering, IEEE Transactions on,* vol. 53, pp. 1440-1445, 2006.

[53] O. Piccin, B. Bayle, B. Maurin, and M. de Mathelin, "Kinematic modeling of a 5-DOF parallel mechanism for semi-spherical workspace," *Mechanism and Machine Theory,* vol. In Press, Corrected Proof.

[54] M. J. H. Lum, J. Rosen, M. N. Sinanan, and B. Hannaford, "Kinematic optimization of a spherical mechanism for a minimally invasive surgical robot," in *Robotics and Automation, 2004. Proceedings. ICRA '04. 2004 IEEE International Conference on*, 2004, pp. 829-834 Vol.1.

[55] D. S. Minhas, J. A. Engh, M. M. Fenske, and C. N. Riviere, "Modeling of needle steering via duty-cycled spinning," in *Conf Proc IEEE Eng Med Biol Soc*, 2007, pp. 2756-9.

[56] A. T. Tung, B.-H. Park, D. H. Liang, and G. Niemeyer, "Laser-machined shape memory alloy sensors for position feedback in active catheters," *Sensors and Actuators A: Physical,* vol. 147, pp. 83-92, 2008.

[57] B. Davies, "Robotics in minimally invasive surgery," in *Through the Keyhole: Microengineering in Minimally Invasive Surgery, IEE Colloquium on*, 1995, pp. 5/1-5/2.

[58] M. Hayashibe, N. Suzuki, M. Hashizume, K. Konishi, and A. Hattori, "Robotic surgery setup simulation with the integration of inverse-kinematics computation and medical imaging," *Computer Methods and Programs in Biomedicine,* vol. 83, pp. 63-72, 2006.

[59] R. Vijaykumar, K. J. Waldron, and M. J. Tsai, "Geometric Optimization of Serial Chain Manipulator Structures for Working Volume and Dexterity," *The International Journal of Robotics Research,* vol. 5, pp. 91-103, 1986.

[60] K. S. Fu, -, *Robotics : control, sensing, vision, and intelligence* vol. 280227. New York: : McGraw-Hill, 1987.

[61] K. Abdel-Malek, F. Adkins, H.-J. Yeh, and E. Haug, "On the determination of boundaries to manipulator workspaces," *Robotics and Computer-Integrated Manufacturing,* vol. 13, pp. 63-72, 1997.

[62] L. Adhami and E. Coste-Maniere, "Optimal planning for minimally invasive surgical robots," *Robotics and Automation, IEEE Transactions on,* vol. 19, pp. 854-863, 2003.

[63] A. Austad, O. J. Elle, and J. S. Røtnes, "Computer-aided planning of trocar placement and robot settings in robot-assisted surgery," *International Congress Series,* vol. 1230, pp. 1020-1026, 2001.

[64] L. W. Sun and C. K. Yeung, "Port placement and pose selection of the da Vinci surgical system for collision-free intervention based on performance optimization," in *Intelligent Robots and Systems, 2007. IROS 2007. IEEE/RSJ International Conference on*, 2007, pp. 1951-1956.

[65] S. Mitsi, K. D. Bouzakis, D. Sagris, and G. Mansour, "Determination of optimum robot base location considering discrete end-effector positions by means of hybrid genetic algorithm," *Robotics and Computer-Integrated Manufacturing,* vol. 24, pp. 50-59, 2008.

[66] J. Yang, W. Yu, J. Kim, and K. Abdel-Malek, "On the placement of open-loop robotic manipulators for reachability," *Mechanism and Machine Theory,* vol. 44, pp. 671-684, 2009.

[67] B. Siciliano, *Robotics modelling, planning and control*. London :: Springer, 2009.

[68] M. H. David A. Simon, T. Kanade, "Techniques for fast and accurate intrasurgical registration," *Journal of Image Guided Surgery,* vol. 1, pp. 17-29, 1995.

[69] C. Baegert, C. Villard, P. Schreck, and L. Soler, "Multi-criteria trajectory planning for hepatic radiofrequency ablation," *Med Image Comput Comput Assist Interv Int Conf Med Image Comput Comput Assist Interv,* vol. 10, pp. 676-84, 2007.

[70] K. Waldron, "Design of Arms," in *The international Encyclopedia of Robotics* John Wiley and Sonsa, 1988.

[71] K. Jin-Oh and K. Khosla, "Dexterity measures for design and control of manipulators," in *Intelligent Robots and Systems '91. 'Intelligence for Mechanical Systems, Proceedings IROS '91. IEEE/RSJ International Workshop on*, 1991, pp. 758-763 vol.2.

[72] M. J. Tsai and Y. H. Chiou, "Manipulability of manipulators," *Mechanism and Machine Theory,* vol. 25, pp. 575-585, 1990.

[73] T. Yoshikawa, "Manipulability of Robotic Mechanisms," *The International Journal of Robotics Research,* vol. 4, pp. 3-9, June 1, 1985 1985.

[74] O. Miyake, H. Kiuchi, K. Yoshimura, and A. Okuyama, "Urological robotic surgery: preliminary experience with the Zeus system," *Int J Urol,* vol. 12, pp. 928-32, Oct 2005.

[75] N. Abolhassani, R. Patel, and M. Moallem, "Needle insertion into soft tissue: A survey," *Medical Engineering & Physics,* vol. 29, pp. 413-431, 2007.

[76] S. Misra, K. J. Macura, K. T. Ramesh, and A. M. Okamura, "The importance of organ geometry and boundary constraints for planning of medical interventions," *Medical Engineering & Physics,* vol. 31, pp. 195-206, 2009.

[77] B. N. Lee, P. B. Nguyen, S. H. Ong, J. Qin, L. Yang, and C. K. Chui, "Image Processing and Modeling for Active Needle Steering in Liver Surgery," in *Informatics in Control, Automation and Robotics, 2009. CAR '09. International Asia Conference on*, 2009, pp. 306-310.

Appendix: Technical Descriptions of AR Robotic System

Fig A. 1 depicts the implementation of the optimal design for maximum dexterity. The 5 DOF sub-manipulator system located at the distal end is dedicated to multiple needle insertions process and capable of dexterous manipulation.

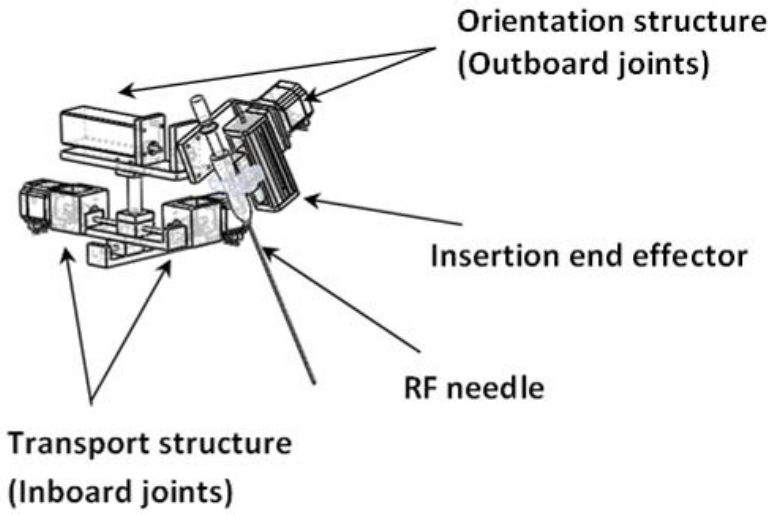

Fig A. 1 Geometric optimal design for maximum dexterity

Fig A. 2 is a technical drawing of the manipulator with various components assembled. The 2 DOF wrist is designed such that the insertion path of the needle is adjustable as shown in Fig A. 3. This facilitates implementation of joint decoupling. The insertion path of the needle can be adjusted to align with the point of intersection of the 2 rotational axes.

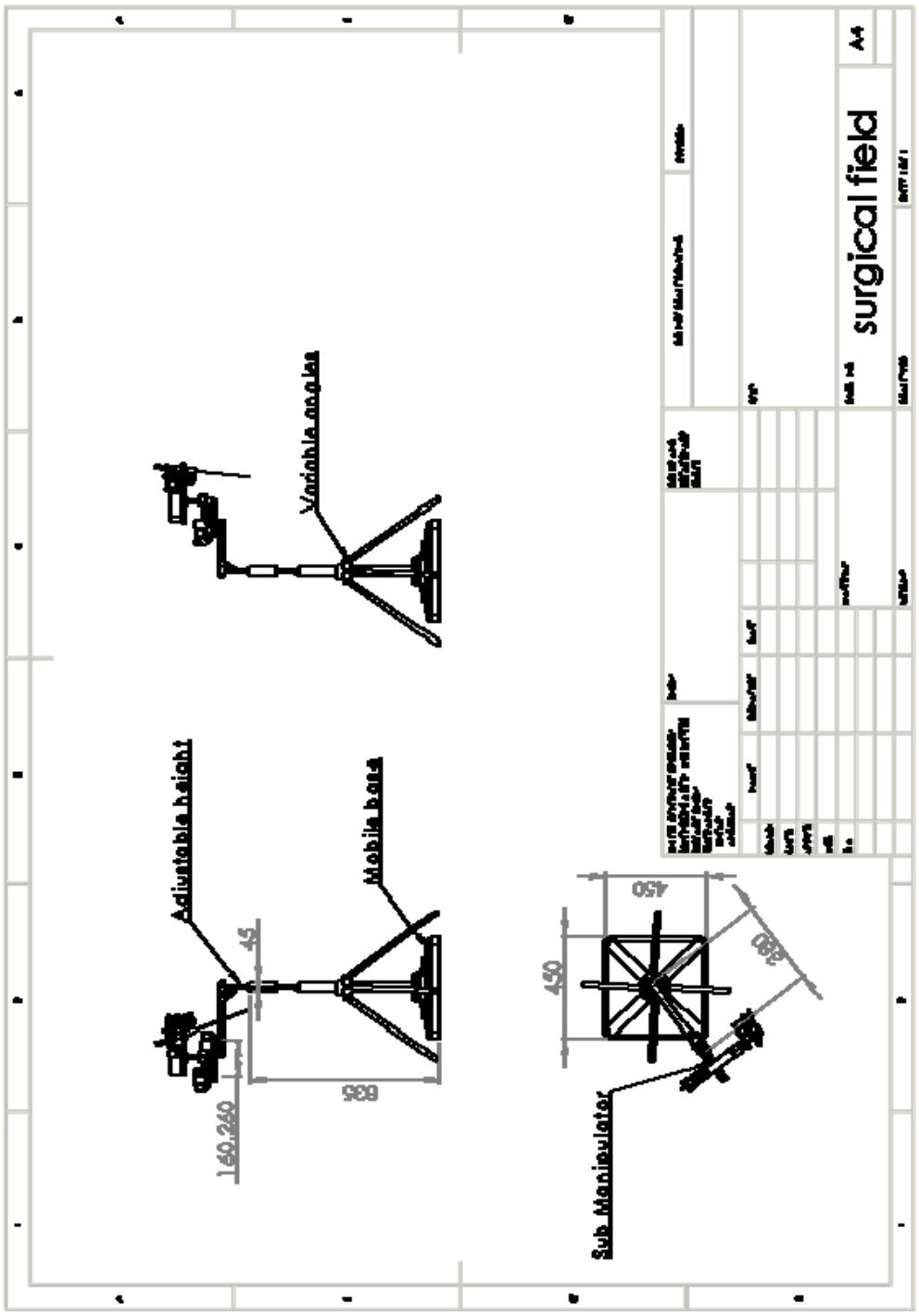

Fig A. 2 Assembly drawing of the robotic needle insertion manipulator

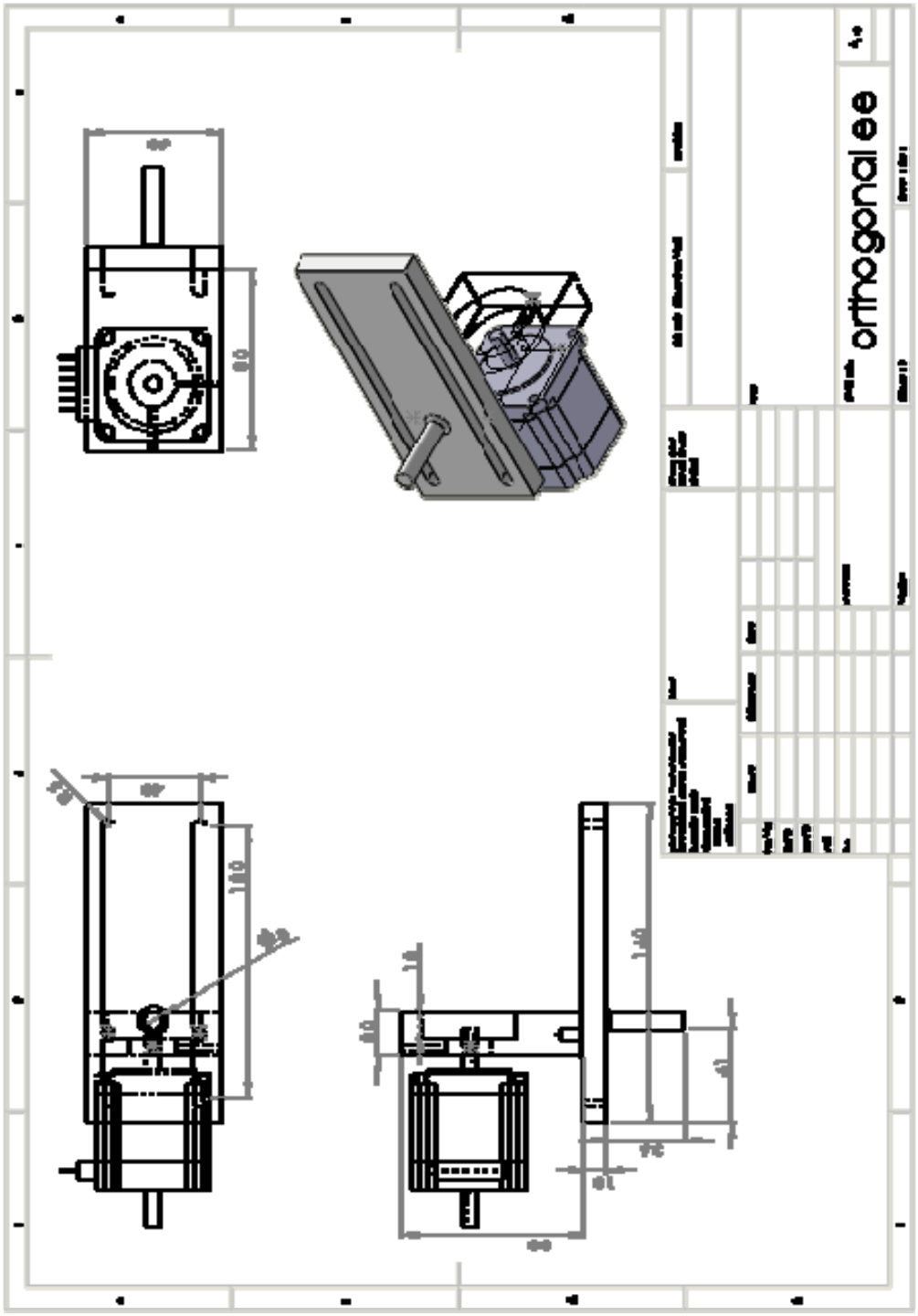

Fig A. 3 Assembly drawing of the orthogonal end effector

Fig A. 4 illustrates the various component of the motorized projector system. The design principle of the mechanism also uses a transport-orientation approach where a motorized x-y stage positions the projector which is also oriented by two joints in a pitch and yaw fashion.

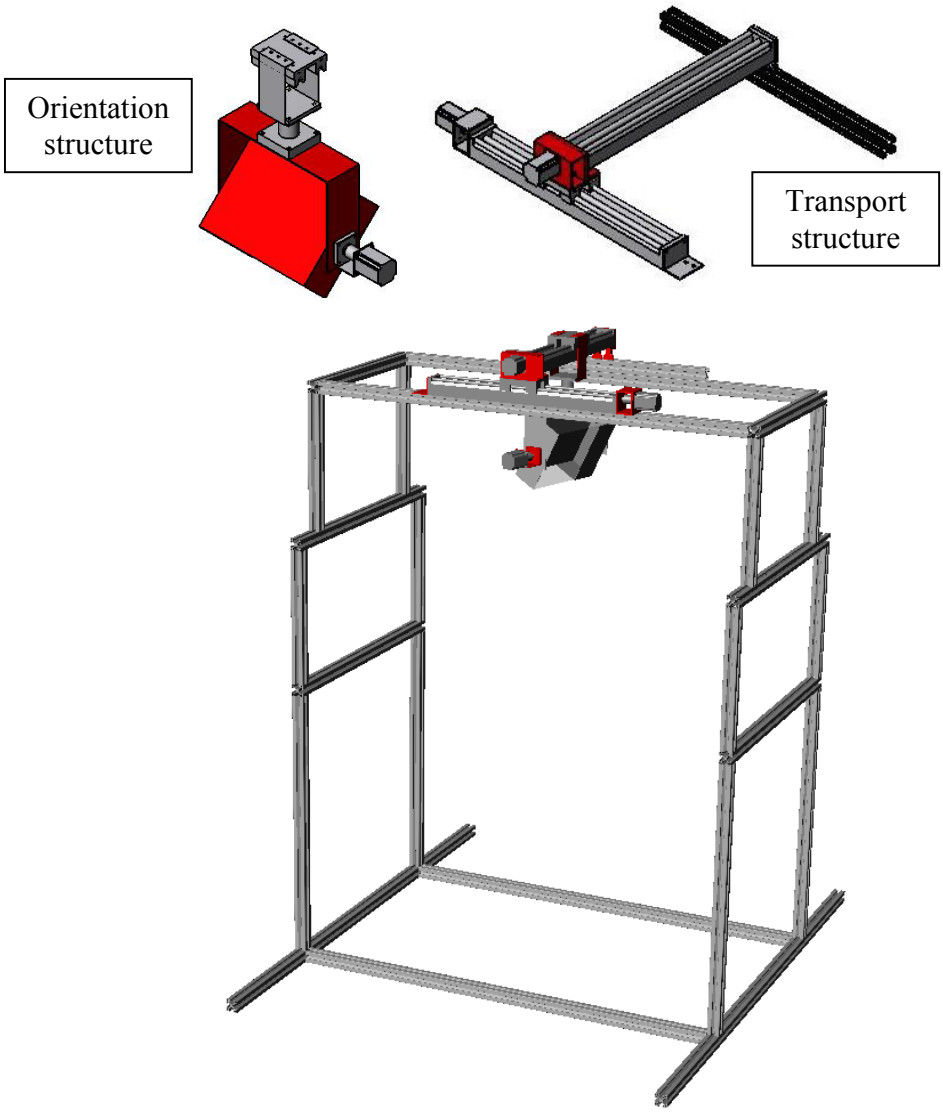

Fig A. 4 Motorized projector system